
Lumped Parameter Whole Body Circulation Modelling

5

Viorel Mihalef, Lucian Itu, Tommaso Mansi,
and Puneet Sharma

Abstract

In this chapter we introduce methodologies for modeling whole-body cardiovascular dynamics. Lumped parameter modeling techniques are employed to model both open-loop and closed-loop dynamics. The main constituents of the model are the pulmonary arterial and venous circulation, the systemic arterial and venous circulation, and the four chambers of the heart. A fully automated parameter estimation framework is introduced, which is based on two sequential steps: first, a series of parameters are computed directly, and, next, a fully automatic optimization-based calibration method is employed to iteratively estimate the values of the remaining parameters. A detailed sensitivity analysis has been performed for identifying the parameters which require calibration. Advanced objectives defined based on slopes and interval of times determined from the measured volume and pressure curves are formulated to improve the overall agreement between computed and measured quantities. Furthermore, methods for modeling subtle influences, e.g. from the KG diaphragm, and pathologic heart valves (stenosed, regurgitant) are introduced.

Parts of Sect. 5.2 have been published before in the paper ‘Model based non-invasive estimation of PV loop from echocardiography’, 36th Annual Inter. Conf. of the IEEE Engineering in Medicine & Biology Society—EMBC 2014, Chicago, USA, August 26–30, pp. 6774–6777, 2014.

V. Mihalef (✉) • T. Mansi • P. Sharma
Medical Imaging Technologies, Siemens Healthcare, 755 College Road,
Princeton, NJ 08540, USA
e-mail: viorel.mihalef@siemens.com

L. Itu
Corporate Technology, Siemens SRL, B-dul Eroilor nr. 3A, Brasov 500007, Romania
Automation and Information Technology, Transilvania University of Brasov,
Mihai Viteazu nr. 5, Brasov 5000174, Romania

The methodology has been validated both for healthy volunteers and for a patient with mild aortic valve regurgitation: a close-agreement between the computed and measured time-varying LV volumes, time-varying LV and aortic pressures, and PV loops has been obtained. This feature is based on research, and is not commercially available. Due to regulatory reasons its future availability cannot be guaranteed.

5.1 Introduction

The capacity of the heart to pump sufficient blood to match its own demands and the demands of the body depends on both intrinsic and extrinsic factors. The modeling of these factors can lead to better approaches for the evaluation and management of cardiac disease, as well as better patient stratification and therapy planning.

In this chapter we present comprehensive whole body circulation models which are able to simulate physiological and pathophysiological characteristics, and quantify the cardiac workload from those characteristics. These methods enable a better understanding of the complex relationship between heart disease and the extra workload on the heart due to various pathologies such as hypertrophy, cardiomyopathy (arrhythmogenic right ventricular cardiomyopathy, isolated ventricular non-compaction, mitochondrial myopathy, dilated cardiomyopathy, restrictive cardiomyopathy, peripartum cardiomyopathy, takotsubo cardiomyopathy, loeffler endocarditis, etc.), mitral regurgitation, aortic stenosis, aortic regurgitation, and hypertension.

Due to the prohibitive computational cost of spatially defined blood flow models (three-dimensional models in particular), whole body circulation models of the cardiovascular system rely heavily on lumped parameter models. These models are based on the analogy between hydraulics and electricity, in the form of RLC circuits (Table 5.1) (Quarteroni et al. 2001).

Closed loop lumped parameter or multiscale models of the cardiovascular system have been introduced in the past (Segers et al. 2003; Korakianitis et al. 2006; Lakin et al. 2007; Kim et al. 2010; Paeme et al. 2011). To model different patient states (steady-state and transient), the cardiovascular model was coupled to a series of models representing the cardiovascular regulatory systems (Fig. 5.1) (Ottesen et al. 2003). The bidirectional exchange of information between the systems leads to a continuous adaptation of the cardiovascular activity and operation.

Table 5.1 Analogy between hydraulics and electricity

Hydraulics	Electricity	
Pressure	Voltage/potential	P
Flow rate	Current	Q
Viscosity	Resistance	R
Inertia	Inductance	L
Compliance	Capacitance	C

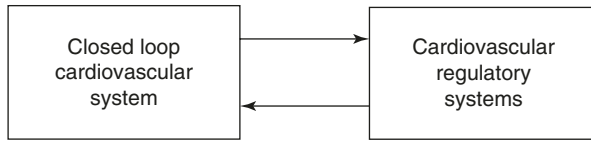


Fig. 5.1 Bidirectional exchange of information between the cardiovascular and the regulatory systems

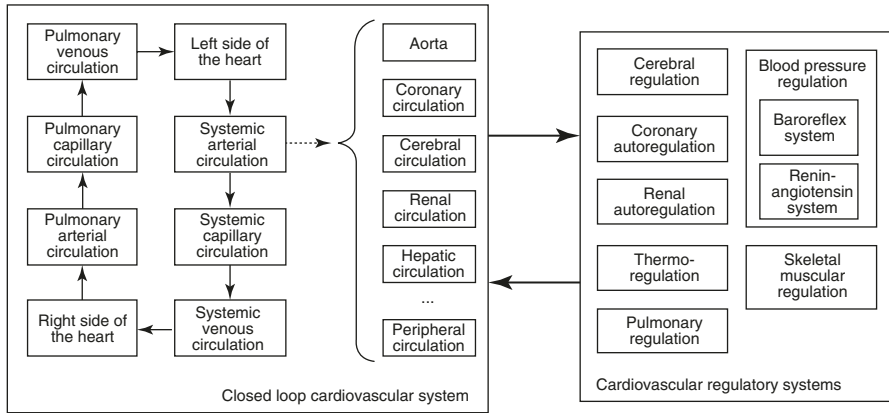


Fig. 5.2 Main components of the cardiovascular system and regulatory systems which act on the cardiovascular system

The closed loop models introduced in the past focus mainly on population average computations in order to quantify the interactions between the different components of the system. No systematic or automatic personalization procedures have been applied. Furthermore, at most one regulatory system was taken into consideration.

In Fig. 5.2 we display a comprehensive model, whereas we have detailed the main components of the systems in Fig. 5.1. The cardiovascular model contains a heart model (left and right side of the heart, each of them with atrium and ventricle), the systemic circulation (arteries, capillaries, veins) and the pulmonary circulation (arteries, capillaries, veins). Figure 5.2 presents a set of possible models for the systemic and pulmonary circulation. Furthermore, various regulatory systems which act on the cardiovascular system are presented in Fig. 5.2 right. The objectives of these systems are to maintain certain levels of blood pressure, flow rate to a certain organ, body temperature, filtration rate, oxygen level in the blood, etc. Specifically, most systems of the body show some degree of autoregulation, the heart and the brain are very sensitive to over- and underperfusion. Coronary autoregulation ensures that the coronary blood supply matches the oxygen demand of the myocardium, both at rest and at exercise (hyperemia), by adapting the resistance of the coronary microvasculature. Cerebral autoregulation also focuses on maintaining an appropriate blood flow to the subtended cerebral tissue.

Furthermore, blood pressure regulation at the systemic level is performed by the baroreflex system, which uses input data provided by the baroreceptors situated mainly in the aortic arch and at the carotid sinuses, and by the renin-angiotensin system which is triggered by pressure and flow receptors in the afferent arterioles of the renal arterial circulation. The renal autoregulation system adapts the resistance of the renal microvasculature in order to maintain the reference glomerular filtration rate.

In the following we first present an open-loop system focusing on the left side of the heart and the systemic circulation, followed by a closed-loop whole body-circulation model.

The concepts and information presented in this chapter are based on research and are not commercially available. Due to regulatory reasons their future availability cannot be guaranteed.

5.1.1 Short-Term Control Mechanisms of the Human Circulatory System

The short term control is mainly performed by the central nervous system (CNS) and includes baroreceptors, mechanoreceptors and chemoreceptors (Guyton 1991). Its goal is to distribute the total flow to the various parts of the body by controlling the heart (heart rate and cardiac contractility) and the vessel constrictions and relaxations. The chemoreceptors react to changes in the concentration of different gases (oxygen, etc.). The baroreceptors react to changes in pressure (the most important receptors of this type are located at the aortic arch and at the carotid sinus). Physiological and historical details regarding the baroreceptor model can be found in Guyton (1991) and Acierno (1994). Mechanoreceptors are mostly found in the atria and pulmonary veins, which are low pressure areas. Out of these three types of receptors, the baroreceptors are the most easily accessible receptors, while the mechanoreceptors are less studied. The baroreceptors play the main role regarding the short term pressure control and have no role in the long term regulation functions.

Two different baroreceptor models have been introduced in Ottesen et al. (2004), which are composed of three parts:

- The afferent part: takes as input the average arterial pressure and outputs the firing rates n ;
- The CNS which takes as input the firing rates and generates the sympathetic and parasympathetic nervous activities (n_s and n_p);
- The efferent part which takes as input the two nervous activities and generates the new values for the controlled parameters.

Based on these three components, a simple and a unified model baroreceptor model are introduced. For the simple model, the sympathetic and parasympathetic activities are computed directly from the mean arterial pressure, by assuming a sigmoidal function:

$$n_s(\bar{p}_{cs}) = \frac{1}{1 + \left(\frac{\bar{p}_{cs}}{\mu}\right)^\nu}, \quad (5.1)$$

$$n_p(\bar{p}_{cs}) = \frac{1}{1 + \left(\frac{\bar{p}_{cs}}{\mu}\right)^{-\nu}}, \quad (5.2)$$

where \bar{p}_{cs} is the measured average pressure, μ is the steady state arterial pressure at the baroreceptors and ν determines the steepness of the sigmoidal curves.

The efferent part is similar for both baroreceptor models and consists of a static and a dynamic component (first order ordinary differential equation). Thus, the generic model, which was adopted, is:

$$\frac{dx_i(t)}{dt} = \frac{1}{\tau_i} \left(-x_i(t) + \alpha_i n_s(\bar{p}_{cs}) - \beta_i n_p(\bar{p}_{cs}) + \gamma_i \right) \quad (5.3)$$

where $x_i(t) = \{HR, E_{max}, R_{ps}, V_{un}, C_v\}$, τ_i represents the transition time until the efferent response i takes effect, α_i and β_i represent the strength of the sympathetic and parasympathetic activity on the response i , whereas γ_i is equal to x_i when no nervous activity is considered. The five controlled quantities are: HR —the heart rate, E_{max} —the maximum contractility of the heart, R_{ps} —the peripheral systemic resistance, V_{un} —the venous unstressed volume and C_v —the venous compliance.

For the unified baroreceptor model described in Ottesen et al. (2004), the firing rates n are computed separately and all three parts of the model are treated separately. Several models have been proposed, which model some or all of the non-linear behavioral aspects of the firing rates (Leaning et al. 1983; Ursino 1999; Ursino 2000; Taher et al. 1988; Ottesen 1997).

When analyzing Eq. (5.3) from the point of view of control theory, it follows that it represents a controller of type PT1 (proportional controller with first order phase lag). Hence, when the hemodynamic conditions change and as a consequence, the average pressure changes, the controllers will counteract this change, but since no integrative component is present in the controller, an error between the reference pressure μ and the measured pressure will appear once the system is perturbed.

The baroreceptor model has been coupled to multiscale model of the human circulation in Kim et al. (2010) and the results have shown that indeed, once a perturbation appears, the average arterial pressure does not reach its previous value.

In a different study (Coogan et al. 2011) a patient-specific simulation, performed for the evaluation of aortic coarctation, was described. In order to match the patient-state as close as possible, the mean average pressure was tuned so as to be identical to the non-invasively measured one. A simple heart model, based on varying elastance, was coupled at the inlet of the aorta and the average aortic pressure was controlled through the left atrial pressure (only the arterial part was modeled).

5.1.2 Coronary Autoregulation

Autoregulation is control mechanism which acts locally and which is independent from the central nervous system. Thus, dilation and contraction of vessels may appear as a consequence of moderate changes in flow rate or pressure (Guyton 1991; Tortora and Anagnostakos 1990). Autoregulation is mainly performed through smooth muscles which surround the vessels (Ganong 1975). In the following we will refer specifically to the coronary autoregulation, since the focus of the current work lies on the simulation and control of the coronary circulation.

Coronary autoregulation plays an important role in stenosed coronary tree at rest state. Its goal is to maintain a certain level of blood flow, given by the myocardial oxygen demand, to the microvascular beds perfused by arteries which contain stenosis. Through autoregulation, the microvascular resistances are decreased so as to eliminate the effect of the stenosis which introduce additional resistances along the epicardial vessels. During hyperemia, the microvascular resistances are already minimal and cannot be decreased further through autoregulation.

One of the most comprehensive studies regarding coronary flow has been described in Miyashiro and Feigl (1995), where both feedforward and feedback mechanism have been used to model coronary autoregulation. Thus α -receptor mediated vasoconstriction and β -receptor mediated vasodilation are modeled through feedforward loops. The feedforward vasodilation generated by the β -receptors appears in order to meet the oxygen demand, but also a feedback loop is necessary in order to obtain a high level of accuracy for the control mechanism. The feedback loop uses as error signal the coronary venous partial pressure of CO_2 and the coronary venous partial pressure of O_2 .

Different experiments have shown that when only the feedback loop is active, the delay of the regulation is higher and overshoot appears, while when the feedforward mechanisms are activated the response is much faster and no overshoot is present. Also, it has been shown the α -receptor mediated vasoconstriction increases the errors and decreases the accuracy of the flow response.

The detailed mechanism which determines a good match between myocardial oxygen consumption and coronary blood flow is not completely known. Several other models have been proposed which use the partial venous pressure of O_2 as the error signal for the metabolic feedback loop (Dankelmann et al. 1992; Drake-Holland et al. 1984). Additionally, other factors intervene like flow-dependent coronary vasodilation induced by endothelium-derived factor (which is a positive feedback flow mechanism) or the myogenic response.

5.2 Non-invasive Estimation of the Left Ventricular Pressure-Volume Loop

The left ventricular pressure-volume (PV) loop represents an efficient tool for understanding and characterizing cardiac function. It contains information regarding stroke volume, cardiac output, ejection fraction, myocardial contractility, cardiac

oxygen consumption, and other important measures of the heart and the systemic circulation. For example, the extent of ventricular remodeling, the degree of ventricular-arterial mismatching (Burkhoff 2013), and the left ventricular end-diastolic pressure-volume relationship (Spevack et al. 2013) represent strong predictors of congestive heart failure. Pathologies such as left ventricular hypertrophy, dilated cardiomyopathy, aortic and mitral valve stenosis, and regurgitation (Hall 2011) are manifested in the PV-loop. Hence, a method for an efficient estimation of the PV loop would represent a powerful diagnostic tool for clinicians. Medical imaging modalities such as MRI, CT, and echocardiography can be used to estimate the time-varying LV volume through the heart cycle in a non-invasive manner, which can then be combined with an invasive measurement of LV pressure to obtain the PV loop (van Slochteren et al. 2012).

In the following, we introduce a model-based approach for the non-invasive estimation of left ventricular, patient-specific PV loops: a lumped parameter circulation model is personalized using a two step parameter estimation framework (Itu et al. 2014). The input data required for the model personalization are acquired through routine non-invasive clinical measurements and echocardiography.

5.2.1 Lumped Parameter Model

The lumped parameter circulation model employed herein is displayed in Fig. 5.3. It comprises three main components: venous pulmonary circulation, the left heart and the systemic circulation. For the venous part of the pulmonary circulation, we use a model composed of a resistance (R_{pulVen}) and compliance (C_{pulVen}):

$$C_{pulVen} \frac{dP_{LA}}{dt} = Q_{C-pulVen}, \quad (5.4)$$

$$Q_{pulVen} = Q_{C-pulVen} + Q_{LA-in}, \quad (5.5)$$

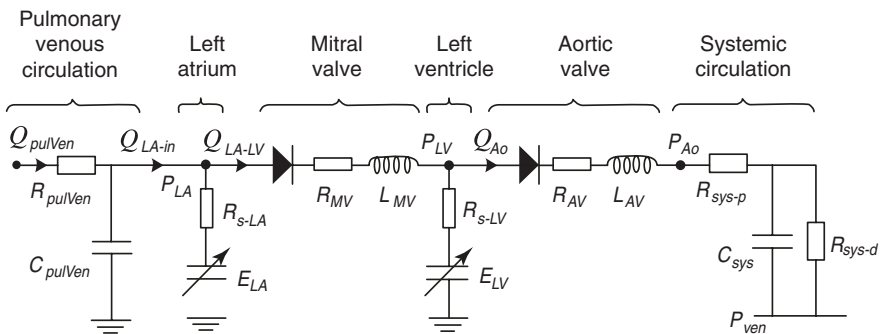


Fig. 5.3 Lumped parameter model representing the venous pulmonary circulation, the left heart and the systemic circulation (Itu et al. 2014)

where the venous pulmonary flow rate (Q_{pulVen}) is considered to be constant in time.

The left heart model has four components: left atrium (LA), mitral valve, left ventricle (LV) and aortic valve. We use a time-varying elastance model for the LA and the LV (Suga 1971):

$$P(t) = E(t) \cdot (V(t) - V_0) - R_s Q(t) \quad (5.6)$$

where E is the time-varying elastance, V is the cavity volume, V_0 is the dead volume of the cavity, and R_s is a source resistance which accounts for the dependence between the flow and the cavity pressure (Shroff et al. 1985) ($R_s = K_s E(t) (V(t) - V_0(t))$, K_s —constant). The cavity volume is equal to:

$$dV / dt = Q_{in} - Q_{out}, \quad (5.7)$$

where Q_{in} represents the inlet flow rate into the cavity and Q_{out} represents the outlet flow rate from the cavity. The mitral valve and the aortic valve are modeled using a resistance, an inductance and a diode to simulate the closure and the opening of the valve (Mynard et al. 2012). When the valve is open, the following relationship holds:

$$P_{in} - P_{out} = R_{valve} \cdot Q + L_{valve} \cdot dQ / dt, \quad (5.8)$$

where P_{in} and P_{out} represent the pressures at the inlet and respectively the outlet of the valve. When the valve is closed, the flow rate through the valve is set to zero. Each valve opens when P_{in} becomes greater than P_{out} , and closes when the flow rate becomes negative. A three-element Windkessel model is used for the systemic circulation, represented by the following relationship between instantaneous flow and pressure.

$$\frac{dP_{Ao}}{dt} = R_{sys-p} \frac{dQ_{Ao}}{dt} - \frac{P_{Ao} - P_{ven}}{R_{sys-d} \cdot C_{sys}} + \frac{Q_{Ao} (R_{sys-p} + R_{sys-d})}{R_{sys-d} \cdot C_{sys}}, \quad (5.9)$$

where R_{sys-p} and R_{sys-d} are the proximal and distal resistances respectively, C_{sys} is the compliance, and P_{ven} is the venous pressure. A total of nine equations are obtained, which are solved implicitly using the forward Euler time integration scheme.

5.2.2 Parameter Estimation Framework

To compute patient-specific left ventricular PV loops using the lumped parameter model, the parameters of the model are personalized. The model personalization framework consists of two sequential steps. First, a series of parameters are computed directly, and next, a fully automatic optimization-based calibration method is employed to estimate the values of the remaining parameters, ensuring that the

Table 5.2 List of patient-specific input parameters

Input	Source
Systolic blood pressure (SBP)	Cuff measurement (arms)
Diastolic blood pressure (DBP)	Cuff measurement (arms)
Heart rate (HR)	Routine measurement
Ejection fraction (EF)	Echocardiography
End-diastolic volume (EDV)	Echocardiography

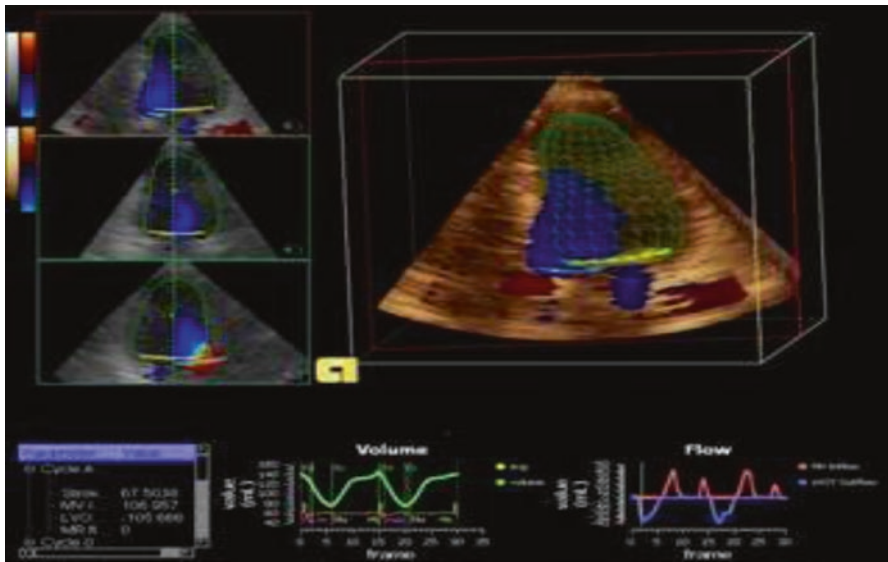


Fig. 5.4 Image acquired through echocardiography illustrating the steps required to extract the end-diastolic volume and the ejection fraction (Itu et al. 2014)

personalized computations match the measurements. Table 5.2 lists the patient-specific input parameters used in the current study, together with their source. Figure 5.4 displays an image acquired through echocardiography, illustrating the steps required for extracting the last two quantities from Table 5.2.

During the first step of the parameter estimation framework, the mean arterial pressure (MAP) is determined:

$$MAP = DBP + \left[\frac{1}{3} + (HR \cdot 0.0012) \right] \cdot (SBP - DBP). \tag{5.10}$$

Then, the end-systolic volume is computed:

$$ESV = EDV \cdot (1 - EF) / 100. \tag{5.11}$$

Next, the stroke volume is determined:

$$SV = EDV - ESV, \tag{5.12}$$

and the average aortic flow rate is computed:

$$\overline{Q_{Ao}} = SV \cdot 60 / HR. \quad (5.13)$$

Finally, the total systemic resistance, as well as the proximal and distal components, are determined:

$$\begin{aligned} R_{sys-t} &= (MAP - P_v) / \overline{Q_{Ao}}, \\ R_{sys-p} &= \rho \cdot R_{sys-t}; \quad R_{sys-d} = (1 - \rho) \cdot R_{sys-t}, \end{aligned} \quad (5.14)$$

where ρ is the proximal resistance fraction. Since the lumped model is used for a pulsatile steady-state computation, the average inlet flow rate (Q_{pulVen}) is equal to the average outlet flow rate, given by Eq. (5.13). Hence:

$$Q_{pulVen} = \overline{Q_{Ao}}. \quad (5.15)$$

The normalized elastance curve is used for the left ventricle model (Suga 1971), which is denormalized using the minimum and maximum elastance values, and the time at which the maximum elastance is reached. The minimum elastance value is set to 0.08 mmHg/ml, and the time at which the maximum elastance of the left ventricle is reached is computed using $t_{max} = 0.16 T + 0.17$, where T is the period. The maximum elastance value is estimated as described further down. A two-hill function is used to determine the elastance curve for the left atrium, whereas the minimum elastance is set to 0.08 mmHg/ml, the maximum elastance is set to 0.17 mmHg/ml, and the onset of the contraction is set at $0.85 T$ (Mynard et al. 2012).

During the second step of the parameter estimation framework, an optimization-based calibration method is employed to estimate the maximum elastance of the left ventricle model, E_{max-LV} , the dead volume of the left ventricle, V_{0-LV} , and the compliance of the systemic Windkessel model, C_{sys} .

The parameter estimation problem is formulated as a numerical optimization problem, the goal of which is to find a set of parameter values for which a set of objectives are met. Since the number of parameters to be estimated is set equal to the number of objectives, the parameter estimation problem becomes a problem of finding the root for a system of nonlinear equations. To solve the system of equations, we use the dogleg trust region method (Nocedal and Wright 2006). The objectives of the parameter estimation method are formulated based on the systolic and diastolic pressures, and the ejection fraction, leading to the system of nonlinear equations:

$$\mathbf{r} \begin{pmatrix} E_{max-LV} \\ V_{0-LV} \\ C_{sys} \end{pmatrix} = \begin{pmatrix} (SBP)_{comp} - (SBP)_{ref} \\ (DBP)_{comp} - (DBP)_{ref} \\ (EF)_{comp} - (EF)_{ref} \end{pmatrix} = \begin{pmatrix} 0 \\ 0 \\ 0 \end{pmatrix}, \quad (5.16)$$

where, $\mathbf{r}(\mathbf{x})$ is a vector function, called in the following objective function, and \mathbf{x} is the vector of the unknowns, i.e. the parameters to be estimated. Each component of the objective function is formulated as the difference between the computed value of a quantity— $(\bullet)_{comp}$ (determined using the lumped parameter model) and its reference value— $(\bullet)_{ref}$ (determined through measurement). To evaluate the objective function for a given set of parameter values, the lumped parameter model is run exactly once. The details of the parameter estimation framework have been introduced in Chap. 4.

5.2.3 Results

To evaluate the performance of the proposed methodology for the non-invasive estimation of left ventricular PV loops, next we present results for three healthy volunteers. Systolic and diastolic pressure values were acquired using cuff-based measurements and the ejection fraction and end diastolic volumes were estimated from the echocardiography performed at rest state in a horizontal position using the Siemens ACUSON SC 2000 ultrasound system. The computed time-varying pressure profiles and PV loops are displayed in Fig. 5.5.

To perform an initial validation of the methodology, we computed the PV loop for a patient with mild aortic valve regurgitation and compared the results against the invasively determined quantities. Figure 5.6 displays a comparison between model-based computed results and invasively performed measurements. The input data used for the parameter estimation framework were extracted from the invasive measurements as follows: *SBP* was the maximum aortic pressure (181.5 mmHg), *DBP* was the minimum aortic pressure (89.7 mmHg), *EDV* was the maximum LV volume (196.68 ml), *EF* (53.1%) was computed from *EDV* and *ESV*, determined as minimum LV volume (92.26 ml), and *HR* was determined from the period of the time-varying pressure (47 bpm). All these values are matched exactly for the output parameter values: $E_{max-LV} = 0.968$ mmHg/ml, $V_{0-LV} = -88.71$ ml, $C_{sys} = 1.065 \times 10^{-3}$ cm⁴ s²/g. There is a close agreement between the time-varying LV and aortic pressures, time-varying LV volumes, and PV loops. Moreover, the four phases of the cardiac cycle can be clearly identified in the computed results (Fig. 5.6a, b): (1) isovolumetric contraction phase, (2) ventricular ejection phase, (3) isovolumetric relaxation phase, and (4) ventricular filling phase. The mild aortic valve regurgitation can be observed in the PV loop in Fig. 5.6c, where the line corresponding to the isovolumetric relaxation has a slight curvature, and in Fig. 5.6b, during the second part of phase 3, where the LV volume increases slightly. The average execution time for the four volunteers/patients was of 28.9 s on a standard Intel i7 CPU core with 3.4 GHz.

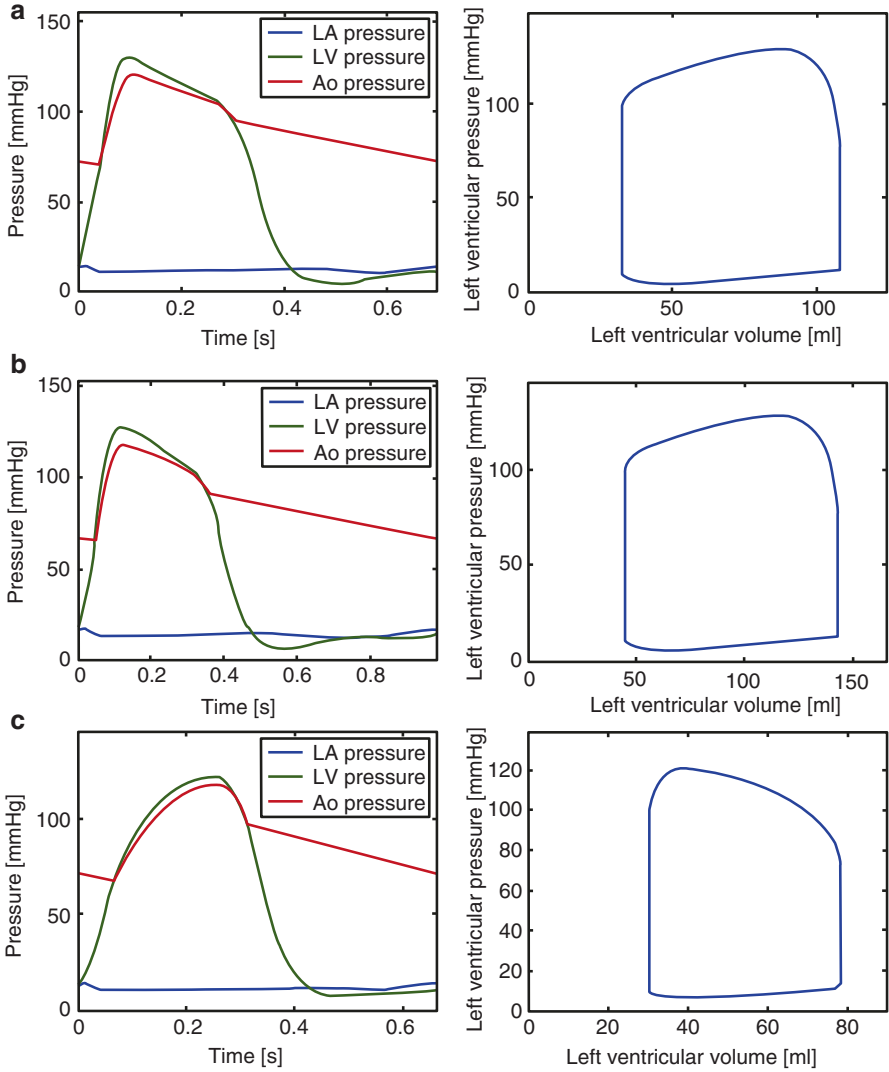


Fig. 5.5 Computed time-varying LA pressure, LV pressure and aortic pressure (*left side*) and PV loops for (a) volunteer 1, (b) volunteer 2, and (c) volunteer 3 (Itu et al. 2014)

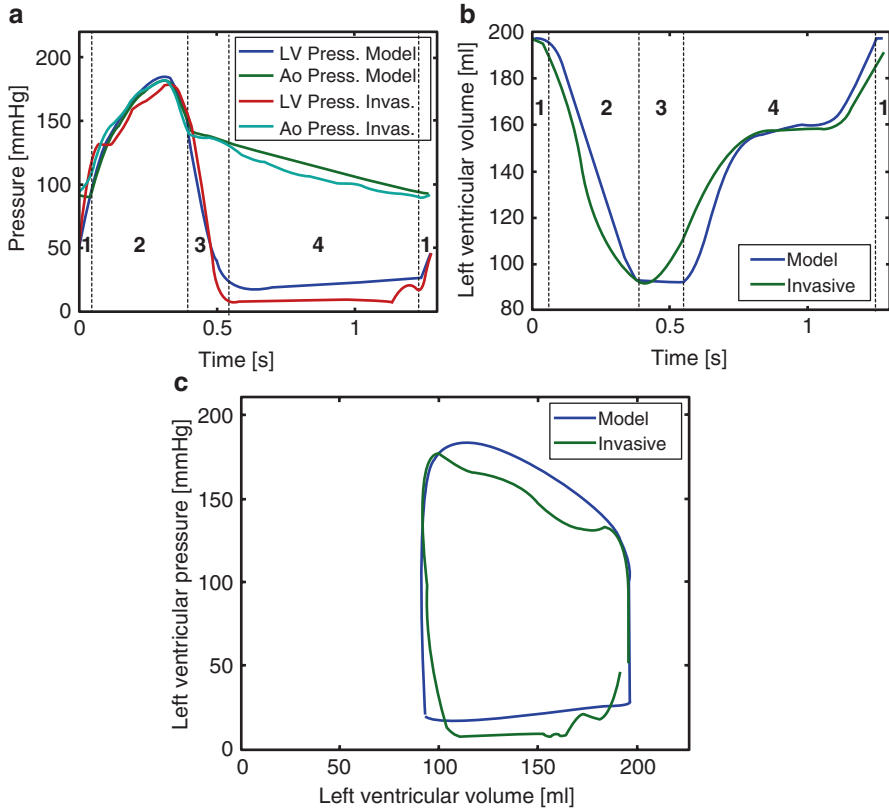


Fig. 5.6 Comparison of model-based computation against invasive measurements, for (a) time-varying left ventricular and aortic pressures, (b) time-varying left ventricular volume, and (c) PV loop (Itu et al. 2014)

5.3 Closed-Loop Whole Body-Circulation Model

The proposed closed-loop whole body-circulation model is displayed in Fig. 5.7.

Time-varying elastance models are used for all four chambers of the heart (Eq. (5.6)):

The models of all four valves (mitral, aortic, tricuspid and pulmonary) of the heart include a resistance, an inertance and a diode (for simulating the opening and the closure of the valve based on the pressure gradient between the two sides of the valve). When the valve is closed the flow across the valve is set to 0. When the valve is open Eq. (5.8) holds:

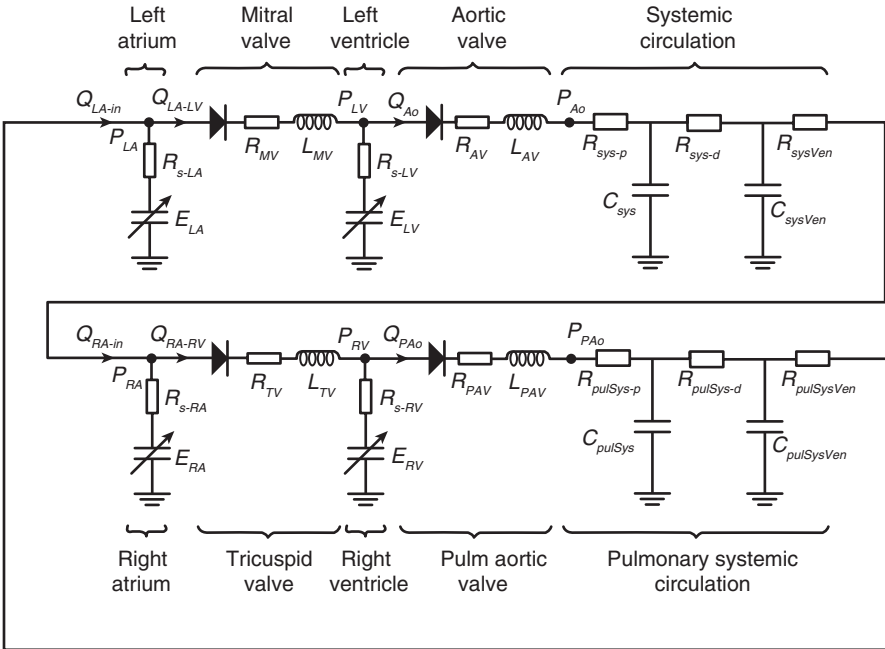


Fig. 5.7 Lumped parameter closed loop model of the cardiovascular system

A three-element Windkessel model is used for the systemic circulation, represented by the following relationship between instantaneous flow and pressure (Eq. (5.9)):

A two-element Windkessel model is used for the systemic venous circulation:

$$\frac{dP_{ven}}{dt} = \frac{Q_{ven}}{C_{sysVen}} - \frac{P_{ven} - P_{RA}}{R_{sysVen} \cdot C_{sysVen}} \tag{5.17}$$

Similar models are used in the pulmonary circulation.

The following parameters may be used as input or output parameters for the closed loop (lumped) models of the cardiovascular system:

- Systolic aortic pressure [mmHg]
- Diastolic aortic pressure [mmHg]
- Heart rate [bpm]
- Ejection fraction [%]
- End-diastolic volume [ml]
- Stroke volume [ml]
- Left ventricular end-systolic pressure [mmHg]
- Left ventricular end-systolic elastance [mmHg/ml]
- Arterial compliance
- $V_{0,*}$ [ml]—dead volume of the * chamber of the heart

- V_{100} [ml]—left ventricular volume corresponding to a left ventricular pressure of 100 mmHg
- Proximal arterial resistance [$\text{g}/(\text{cm}^4 \text{ s})$]
- Distal arterial resistance [$\text{g}/(\text{cm}^4 \text{ s})$]
- Total arterial resistance [$\text{g}/(\text{cm}^4 \text{ s})$]
- Stroke work PV [J]: stroke work determined from computed PV loop
- Normalized stroke work PV [J/ml]: stroke work PV divided by stroke volume
- Stroke work PQt [J]: stroke work determined from computed left ventricular pressure and aortic flow rate
- Normalized stroke work PQt [J/ml]: stroke work PQt divided by stroke volume
- Arterial elastance [mmHg/ml]: computed as end systolic pressure divided by stroke volume
- Arterial ventricular coupling: arterial elastance divided by left ventricular end-systolic elastance

To compute patient-specific hemodynamics, the model in Fig. 5.7 requires personalization. Figure 5.8 displays the overall workflow used for fully automatic model personalization. The first step is to define the metrics of interest: the main output(s) of the model. Herein these are:

- Arterial compliance
- $V_{0,*}$ and V_{100}

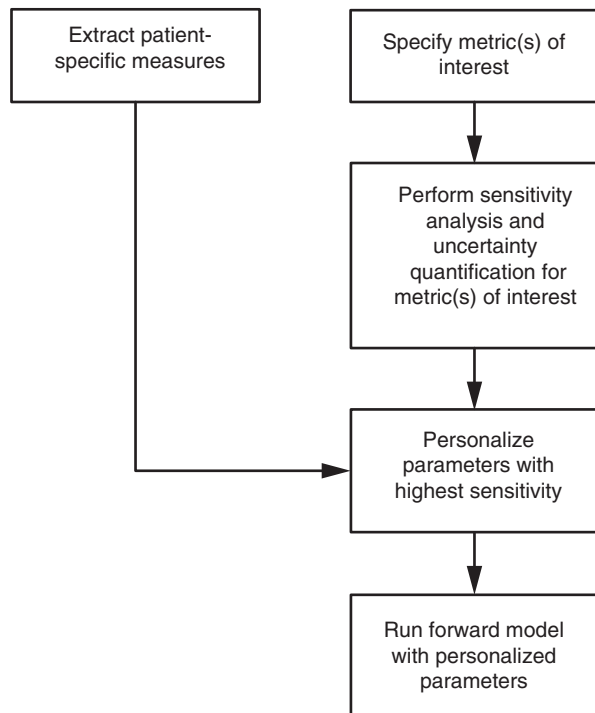


Fig. 5.8 Overall workflow used for personalization

- Proximal, distal and total arterial resistance
- Stroke work
- Arterial elastance
- Arterial ventricular coupling

The next step is to perform a sensitivity analysis to identify the main parameters of the model which affect the outputs of interest. To achieve this, both global sensitivity analysis and uncertainty quantification are performed (based on the stochastic collocation method and polynomial chaos expansion). Once the parameters with the highest influence on the metrics of interest have been identified they are personalized based on patient-specific measures. Herein, these measures are:

- Non-invasive measurements (cuff-based pressures systemic systolic and diastolic pressures, heart rate)
- left and right ventricle volume

Population-average values are used for the parameters which are not personalized. The personalization consists in running a forward model multiple times until the objectives in the model outputs are met.

5.3.1 Local Sensitivity Analysis

The results of a local sensitivity analysis performed with the whole body circulation lumped parameter model are described below. In each test one parameter is modified, while the others are maintained constant. Effects have been analyzed for the LV pressure, LV volume and the systemic arterial pressure.

Figure 5.9 displays the effects of a variation in the initial volume in the LA and the LV on the computed quantities (LV pressure, aortic pressure and LV volume). In open loop models the inlet boundary condition controls the volume of blood in the model, and this value may change from one heart cycle to the next, as the computation progresses from a transient to a steady state. In closed loop models however, the initial volume in the system is maintained from one heart cycle to the next, and hence the initialization of the model with the ‘correct’ amount of blood is crucial.

Figure 5.10 displays the effects of a variation in the maximum elastance of the LV. A lower maximum elastance mainly affects early systole in the LV and aortic pressures, it leads to a slight decrease of the diastolic aortic pressure and to an increase of the LV volume. The lower the maximum elastance, the smaller becomes the stroke volume and, as a result, the levels of the LV volume increases.

Figure 5.11 displays the effects of a variation in the systemic compliance. A lower compliance leads to a higher afterload, and hence to higher LV and aortic pressures, the diastolic aortic pressure decay becomes more prominent (the time constant of the systemic circulation decreases), and the LV volume increases (due to the higher afterload less blood is pumped out of the LV).

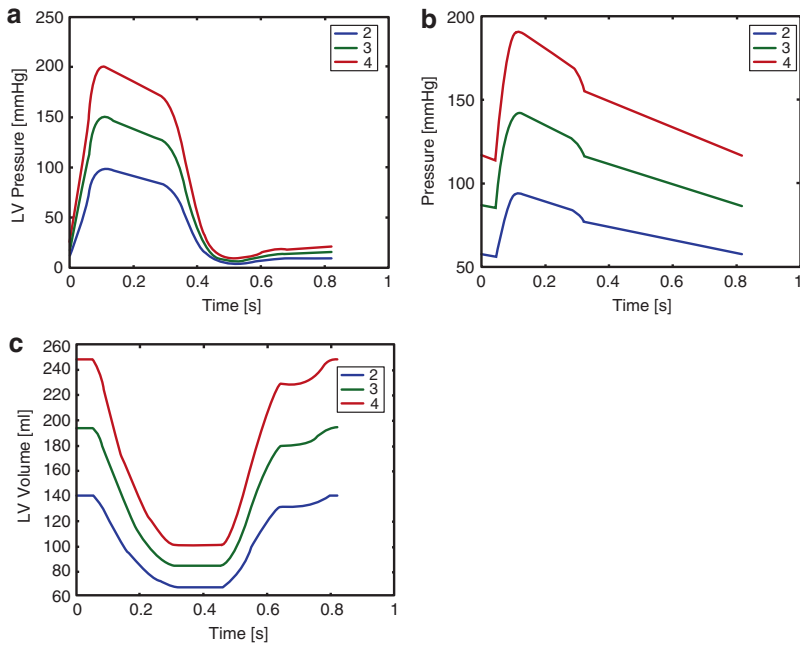


Fig. 5.9 Effect of initial LA and LV volume on (a) LV pressure, (b) aortic pressure, (c) LV volume. A manifold of the patient-specific LV end-diastolic volume is used (2, 3 or 4)

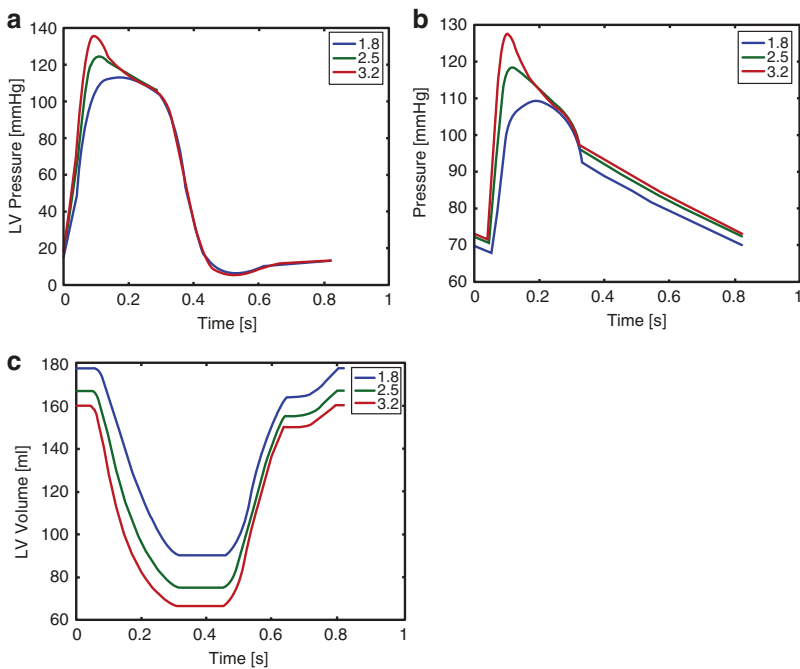


Fig. 5.10 Effect of LV maximum elastance on (a) LV pressure, (b) aortic pressure, (c) LV volume. Elastance is expressed in [mmHg/ml]

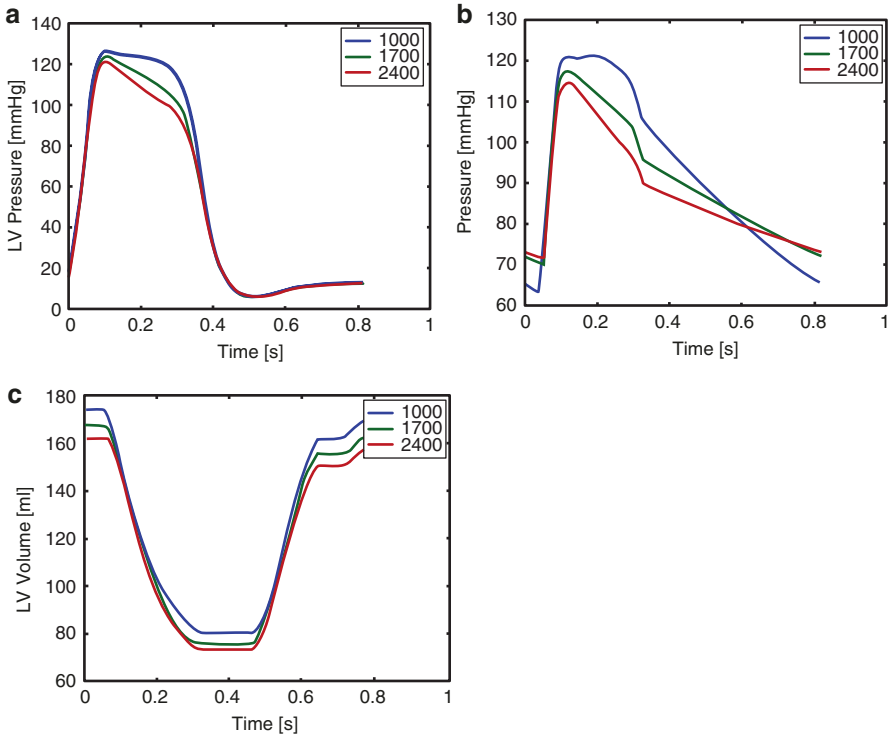


Fig. 5.11 Effect of systemic compliance on (a) LV pressure, (b) aortic pressure, (c) LV volume. Compliance is expressed in $[10^{-6} \text{ cm}^4 \text{ s}^2/\text{g}]$

Figure 5.12 displays the effects of a variation in the dead volume of the LV. LV and aortic pressures are largely unaffected, while the LV volume levels are shifted by a value approximately equal to the variation in the dead volume.

Figure 5.13 displays the effects of a variation of the time when LV elastance is maximum: the systolic period (the ejection time) is increased.

Figure 5.14 displays the effects of a variation in the maximum LA elastance: effects are negligible.

Figure 5.15 displays the effects of a variation in the minimum LA elastance: the filling phase of the LV after the atrial kick is slightly affected.

Figure 5.16 displays the effects of a variation in the LA onset of contraction: the filling phase of the LV after atrial the kick is slightly affected: with later onset, the atrial kick becomes less pronounced.

Figure 5.17 displays the effects of a variation in the LA dead volume. With increasing dead volume LV pressure, aortic pressure, and LV volume are slightly shifted downwards.

Figure 5.18 displays the effects of a variation in the systemic venous compliance. Since the systemic venous compliance is very large and stores a large amount of blood, a decrease of this compliance will lead to higher overall levels of pressure and LV volume.

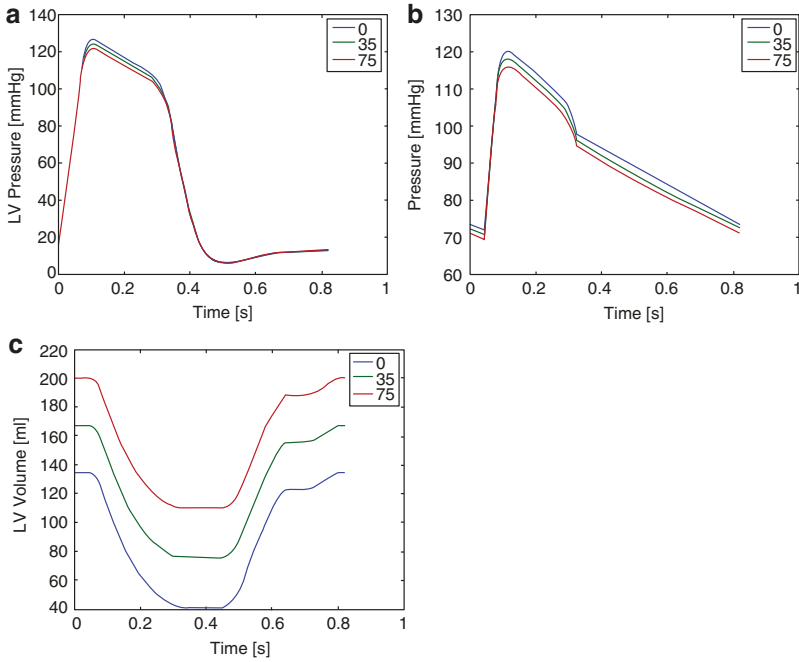


Fig. 5.12 Effect of LV dead volume on (a) LV pressure, (b) aortic pressure, (c) LV volume. Volume is expressed in [ml]

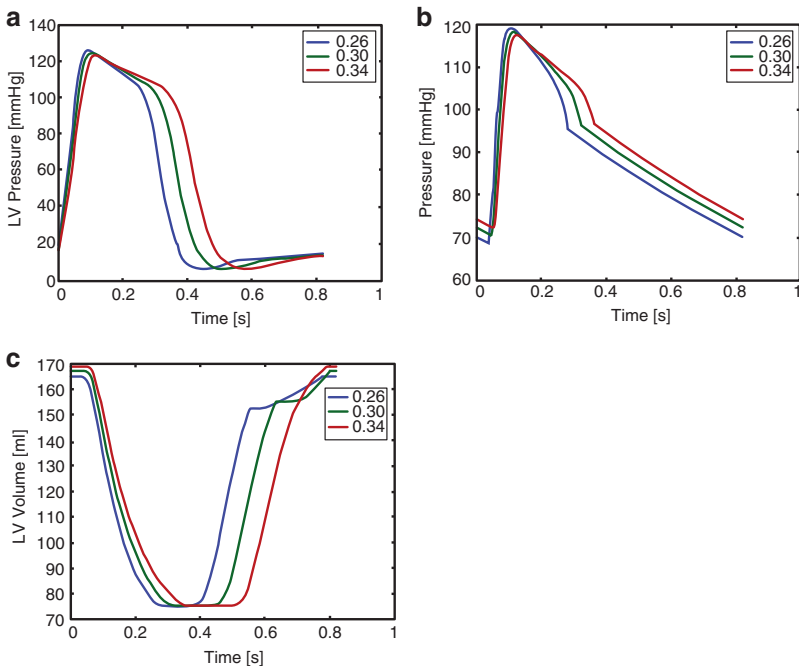


Fig. 5.13 Effect of time when LV elastance is maximum on (a) LV pressure, (b) aortic pressure, (c) LV volume. Time is expressed in [s]

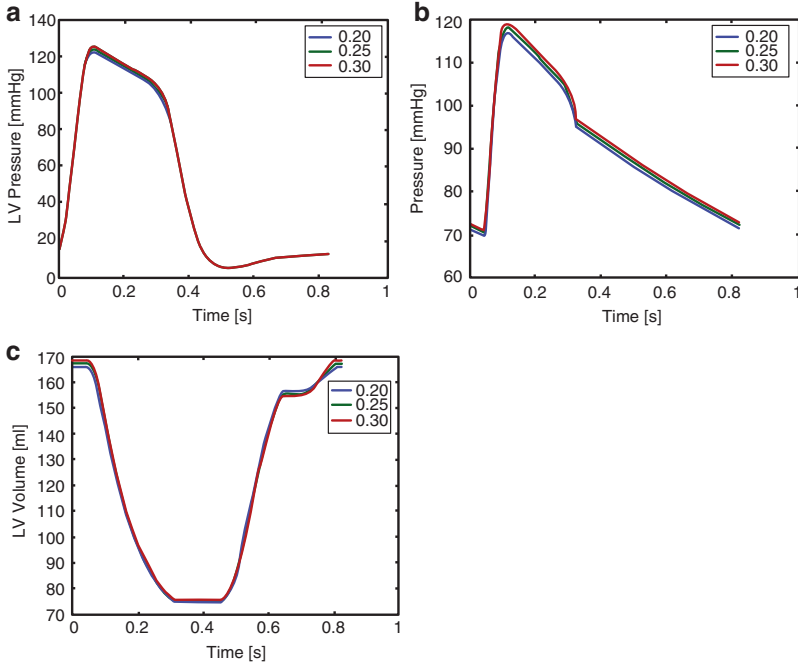


Fig. 5.14 Effect of LA maximum elastance on (a) LV pressure, (b) aortic pressure, (c) LV volume. Elastance is expressed in [mmHg/ml]

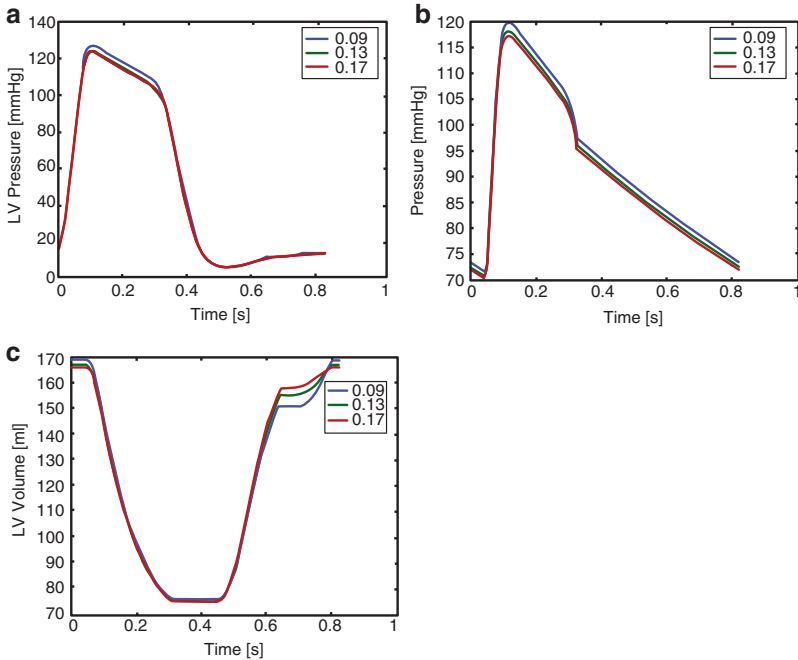


Fig. 5.15 Effect of LA minimum elastance on (a) LV pressure, (b) aortic pressure, (c) LV volume. Elastance is expressed in [mmHg/ml]

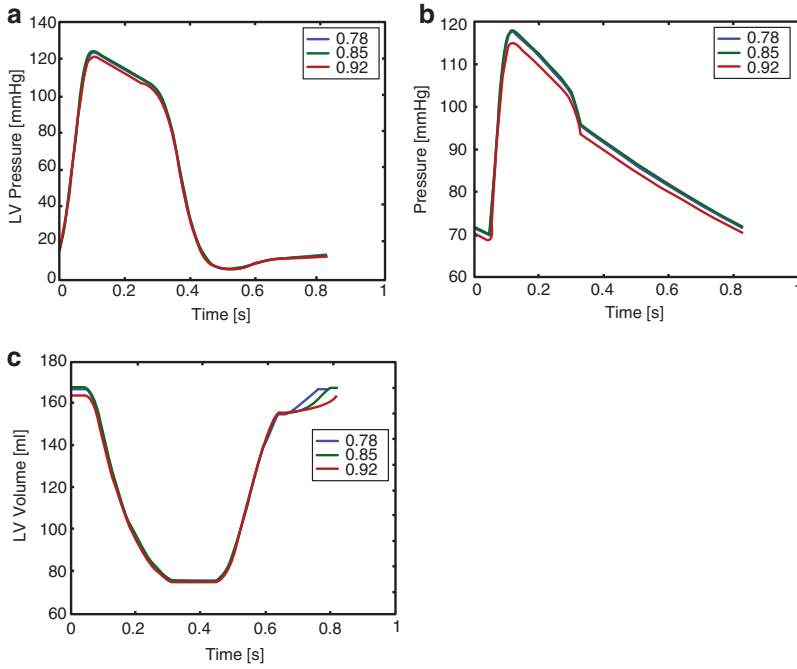


Fig. 5.16 Effect of LA onset of contraction on (a) LV pressure, (b) aortic pressure, (c) LV volume. Moment of onset is expressed relative to the cycle period

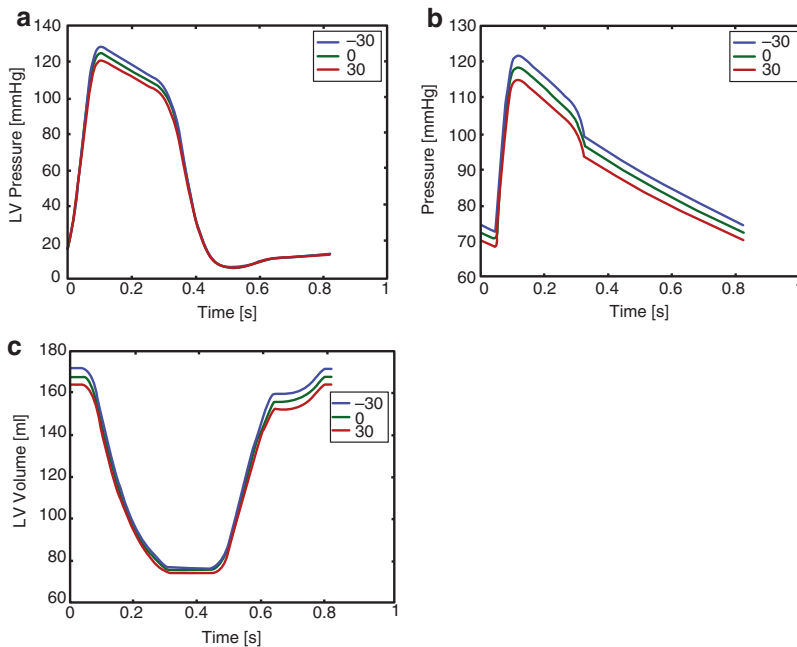


Fig. 5.17 Effect of LA dead volume on (a) LV pressure, (b) aortic pressure, (c) LV volume. Volume is expressed in [ml]

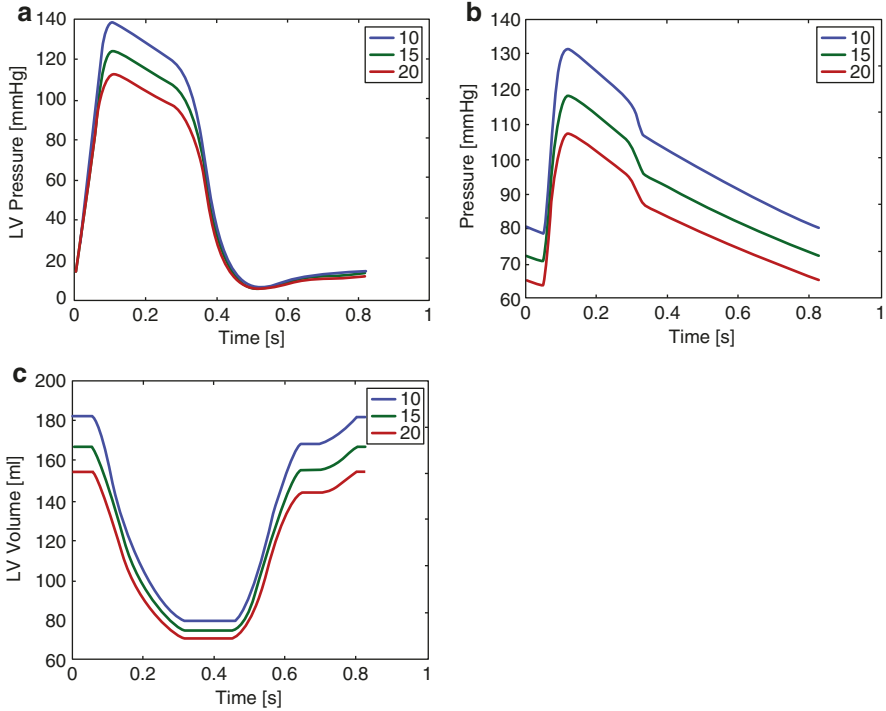


Fig. 5.18 Effect of systemic venous compliance on (a) LV pressure, (b) aortic pressure, (c) LV volume. Compliance is expressed in $[10^{-6} \text{ cm}^4 \text{ s}^2/\text{g}]$

Figure 5.19 displays the effects of a variation in the aortic valve resistance (only a healthy valve is considered): effects are negligible.

Figure 5.20 displays the effects of a variation in the aortic valve inertance (only a healthy valve is considered): effects are negligible.

Figure 5.21 displays the effects of a variation in the mitral valve resistance (only a healthy valve is considered). The mitral valve resistance mainly affects the slope of the ventricular filling phase.

Figure 5.22 displays the effects of a variation in the mitral valve inertance (only a healthy valve is considered). The mitral valve inertance affects the shape of the ventricular filling phase.

Figure 5.23 displays the effects of a variation in the RV maximum elastance. A lower RV maximum elastance leads to a decrease of LV pressure, aortic pressure and LV volume but the effects are overall small.

Figure 5.24 displays the effects of a variation of the time when RV elastance is maximum: effects are negligible.

Figure 5.25 displays the effects of a variation in the dead volume of the RV: the effects are negligible.

Figure 5.26 displays the effects of a variation in the pulmonary aortic resistance: the effects are negligible.

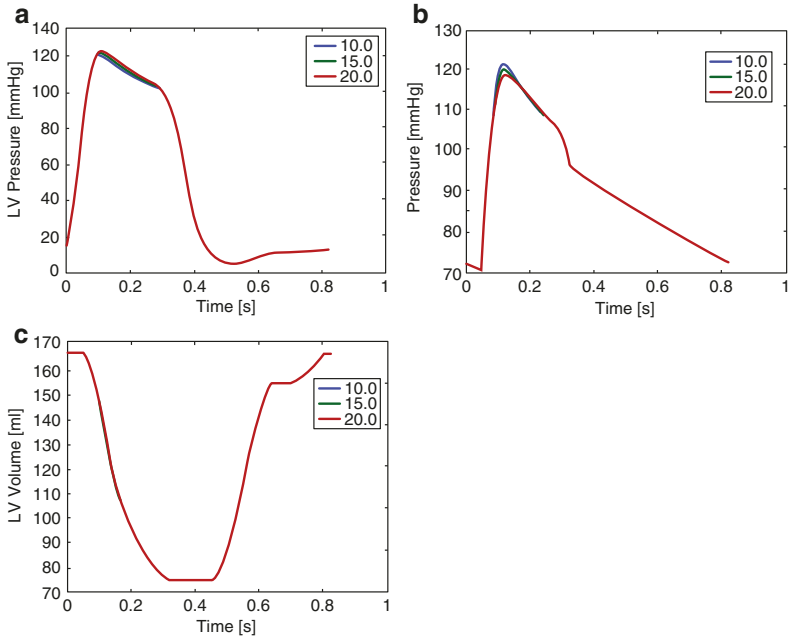


Fig. 5.19 Effect of aortic valve resistance on (a) LV pressure, (b) aortic pressure, (c) LV volume. Resistance is expressed in $[g/(cm^4 s)]$

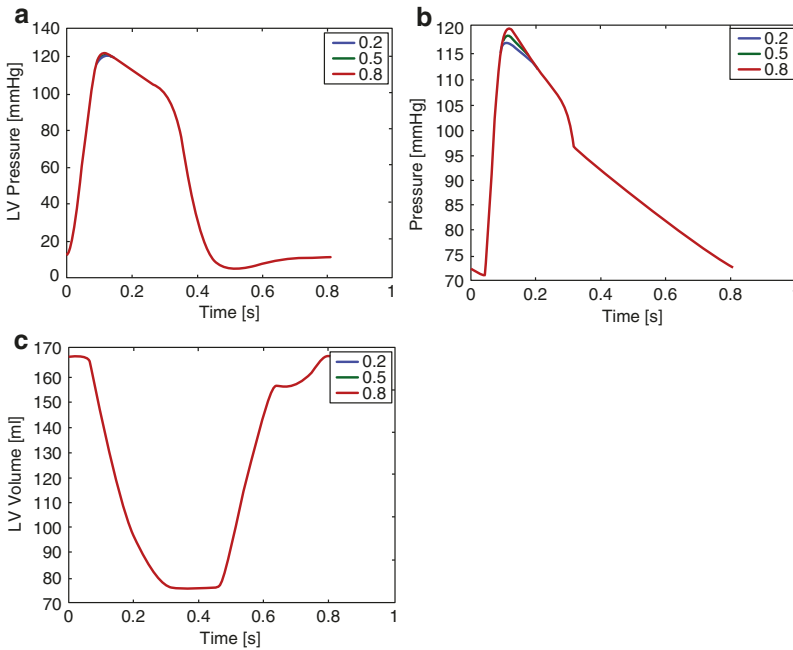


Fig. 5.20 Effect of aortic valve inertance on (a) LV pressure, (b) aortic pressure, (c) LV volume. Inertance is expressed in $[cm^2/s]$

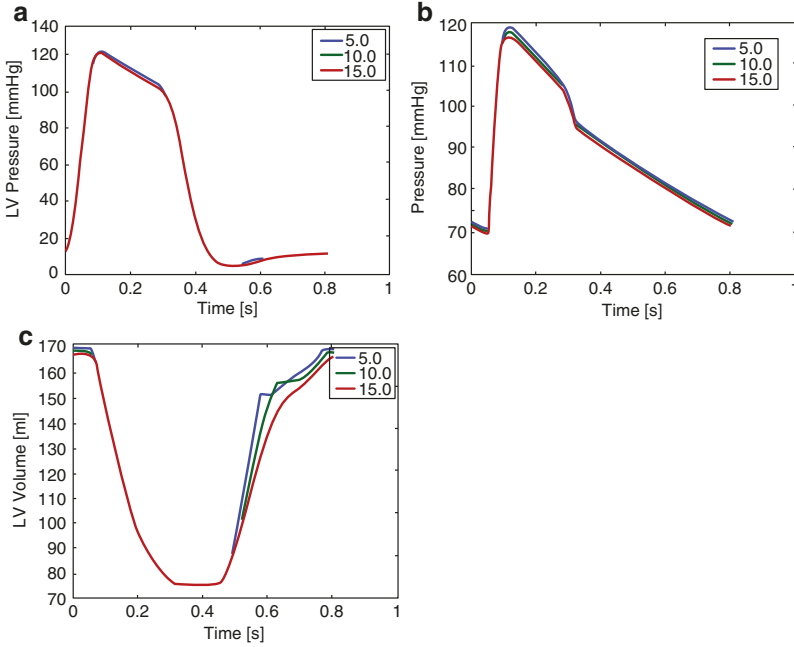


Fig. 5.21 Effect of mitral valve resistance on (a) LV pressure, (b) aortic pressure, (c) LV volume. Resistance is expressed in $\text{g}/(\text{cm}^4 \text{ s})$

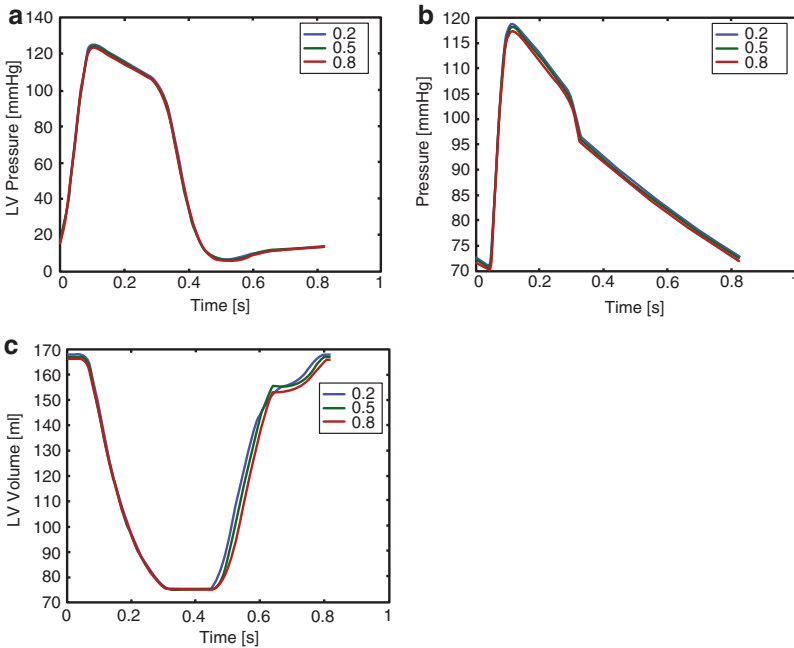


Fig. 5.22 Effect of mitral valve inertance on (a) LV pressure, (b) aortic pressure, (c) LV volume. Inertance is expressed in cm^2/s

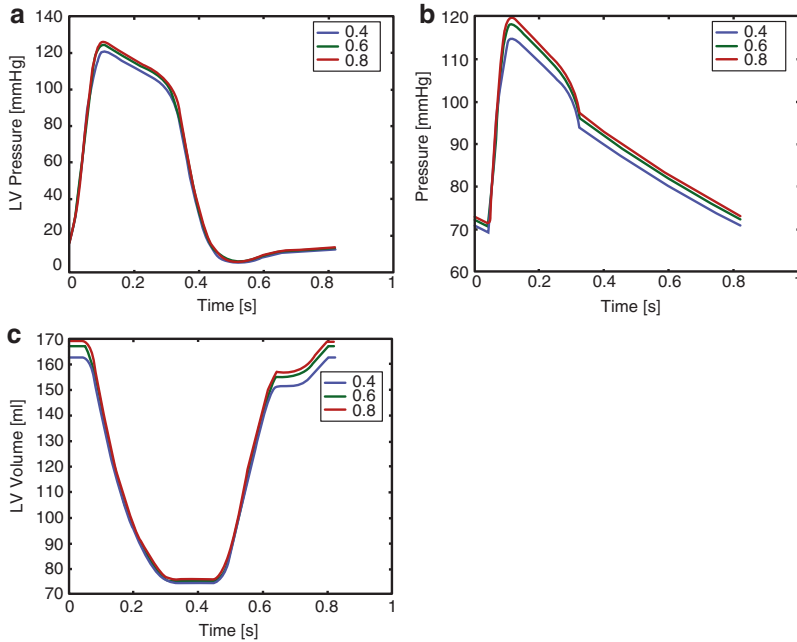


Fig. 5.23 Effect of RV maximum elastance on (a) LV pressure, (b) aortic pressure, (c) LV volume. Elastance is expressed in [mmHg/ml]

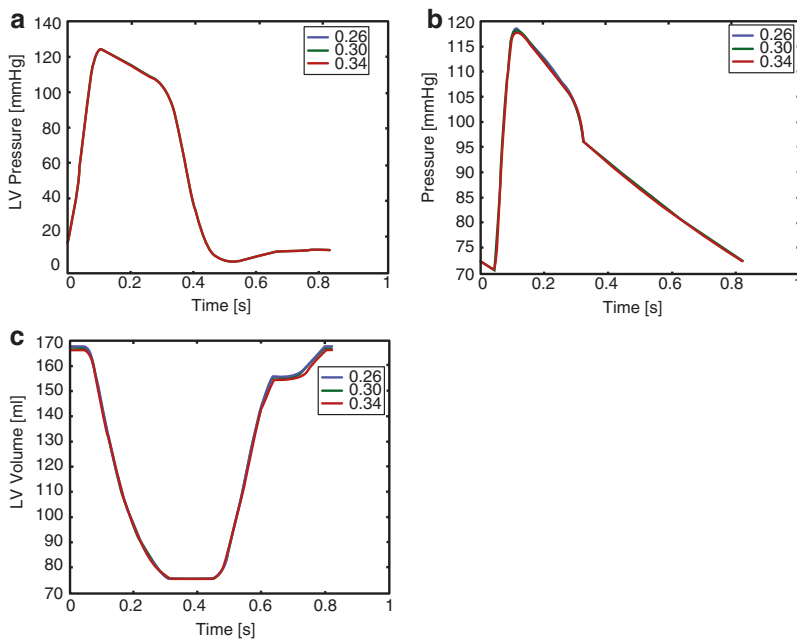


Fig. 5.24 Effect of time when RV elastance is maximum on (a) LV pressure, (b) aortic pressure, (c) LV volume. Time is expressed in [s]

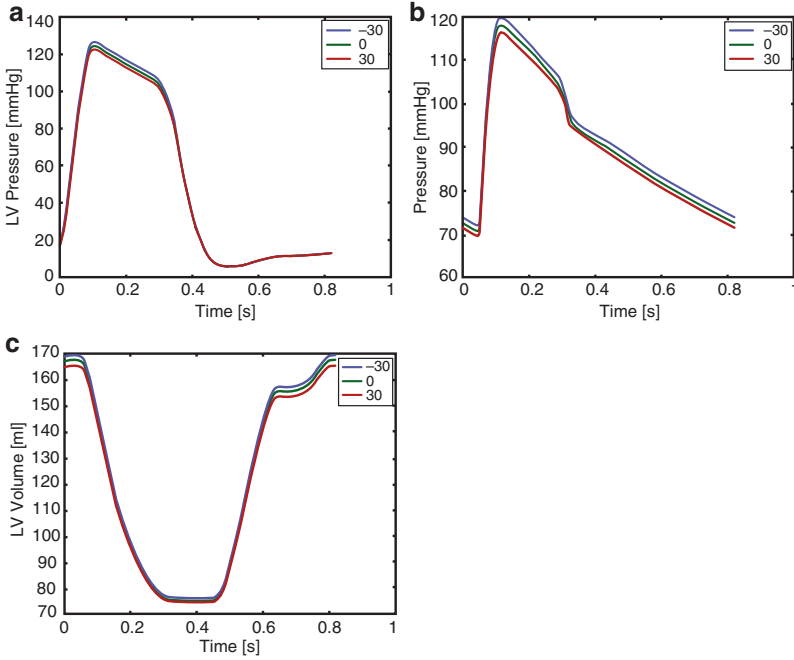


Fig. 5.25 Effect of RV dead volume on (a) LV pressure, (b) aortic pressure, (c) LV volume. Volume is expressed in [ml]

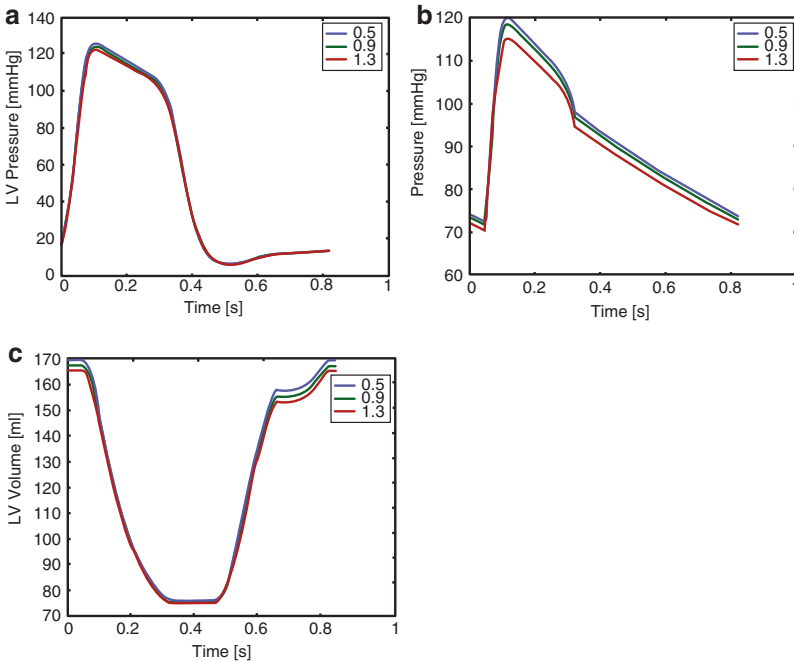


Fig. 5.26 Effect of pulmonary aortic resistance on (a) LV pressure, (b) aortic pressure, (c) LV volume. Resistance is expressed in [g/(cm⁴ s)]

Figure 5.27 displays the effects of a variation in the pulmonary aortic compliance: the effects are negligible.

Figure 5.28 displays the effects of a variation in the pulmonary venous compliance. Since the pulmonary venous compliance is very large and stores a large amount of blood, a decrease of this compliance will lead to higher overall levels of pressure and LV volume.

Figure 5.29 displays the effects of a variation in the pulmonary valve resistance (only a healthy valve is considered): effects are negligible.

Figure 5.30 displays the effects of a variation in the pulmonary valve inertance (only a healthy valve is considered): effects are negligible.

Figure 5.31 displays the effects of a variation in the tricuspid valve resistance (only a healthy valve is considered): effects are negligible.

Figure 5.32 displays the effects of a variation in the tricuspid valve inertance (only a healthy valve is considered):

Figure 5.33 displays the effects of a variation in the heart rate. With lower HR value, the ejection time decreases, but the ratio of systolic to diastolic time increases. Stroke volume decreases slightly. Hence, also the overall LV and aortic pressure level decreases slightly. Note that no autoregulation mechanism is used.

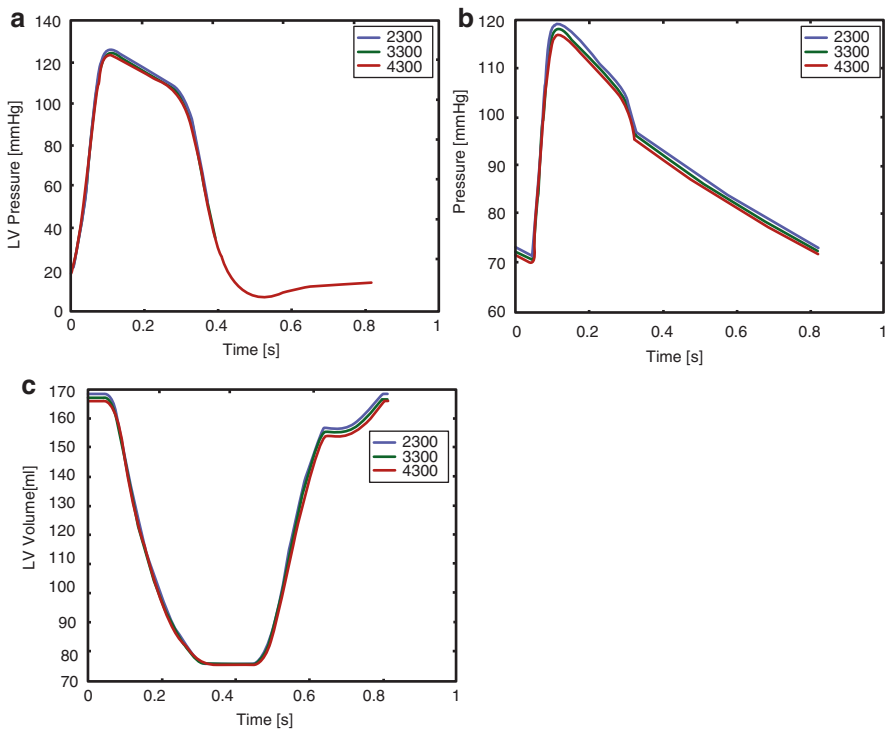


Fig. 5.27 Effect of pulmonary aortic compliance on (a) LV pressure, (b) aortic pressure, (c) LV volume. Compliance is expressed in $[10^{-6} \text{ cm}^4 \text{ s}^2/\text{g}]$

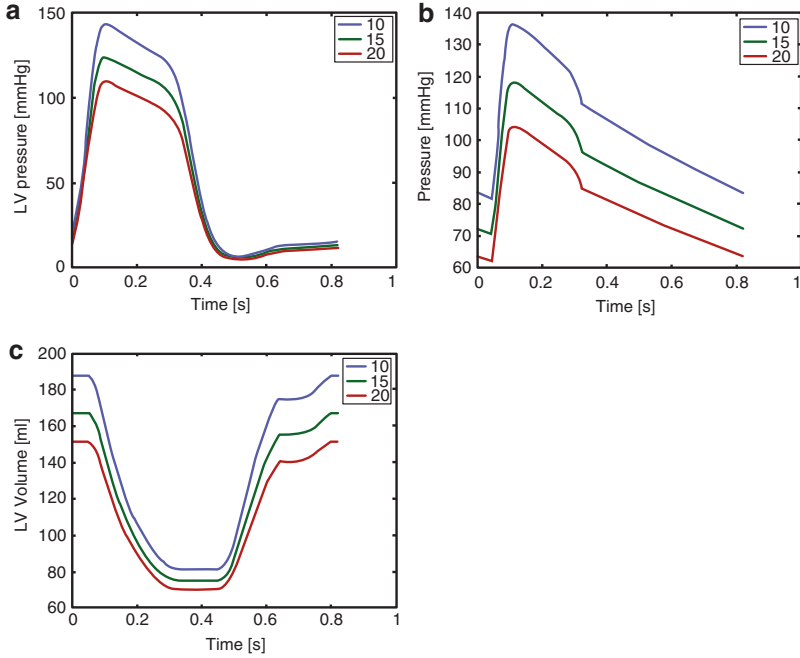


Fig. 5.28 Effect of pulmonary venous compliance on (a) LV pressure, (b) aortic pressure, (c) LV volume. Compliance is expressed in $[10^{-6} \text{ cm}^4 \text{ s}^2/\text{g}]$

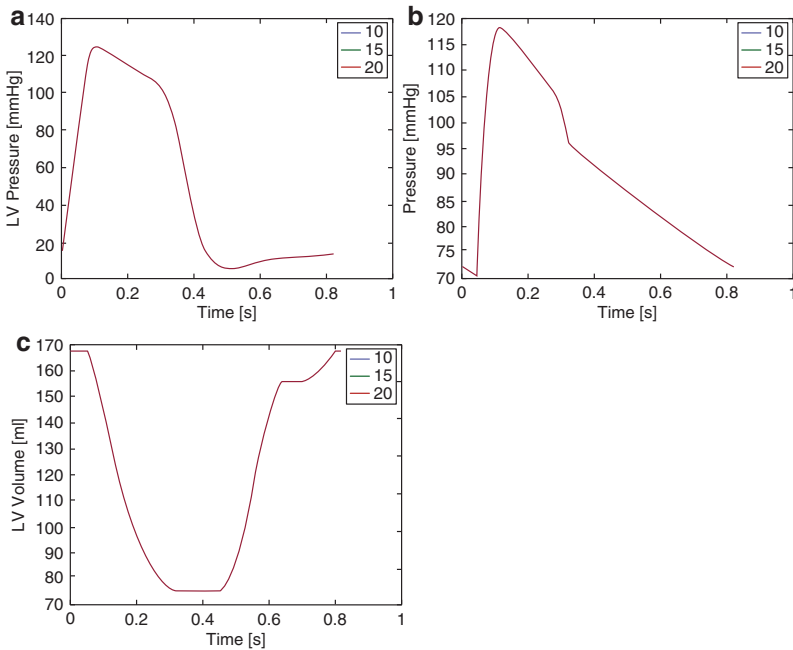


Fig. 5.29 Effect of pulmonary valve resistance on (a) LV pressure, (b) aortic pressure, (c) LV volume. Resistance is expressed in $[\text{g}/(\text{cm}^4 \text{ s})]$

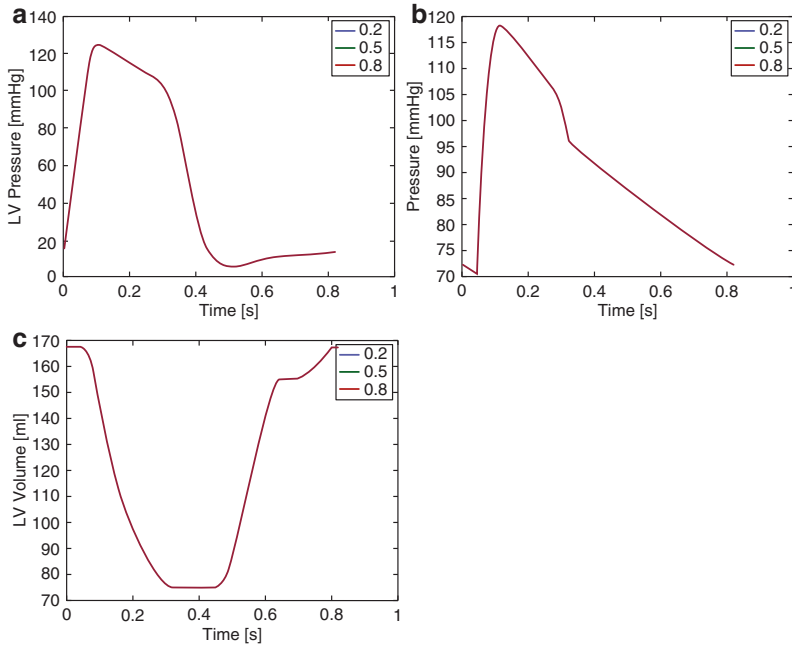


Fig. 5.30 Effect of pulmonary valve inertance on (a) LV pressure, (b) aortic pressure, (c) LV volume. Inertance is expressed in $[cm^2/s]$

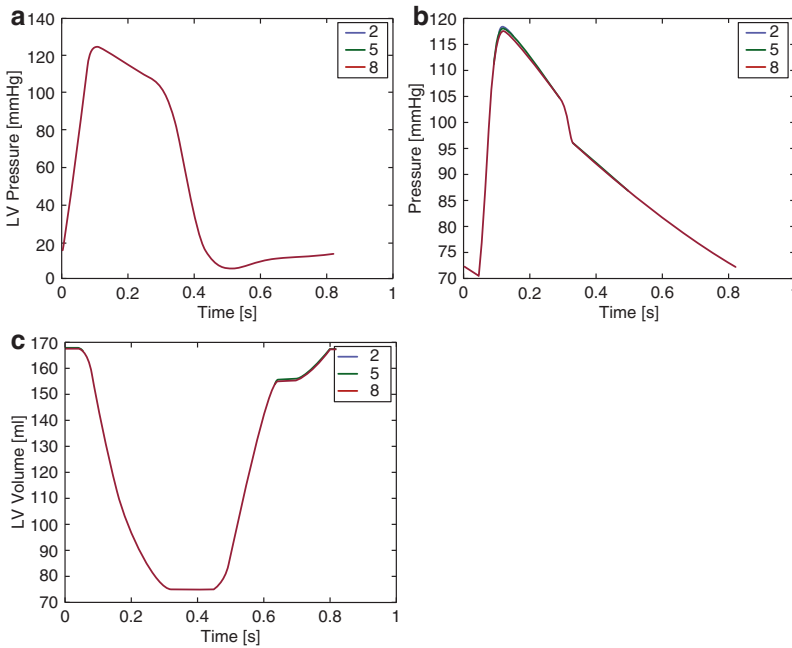


Fig. 5.31 Effect of tricuspid valve resistance on (a) LV pressure, (b) aortic pressure, (c) LV volume. Resistance is expressed in $[g/(cm^4 s)]$

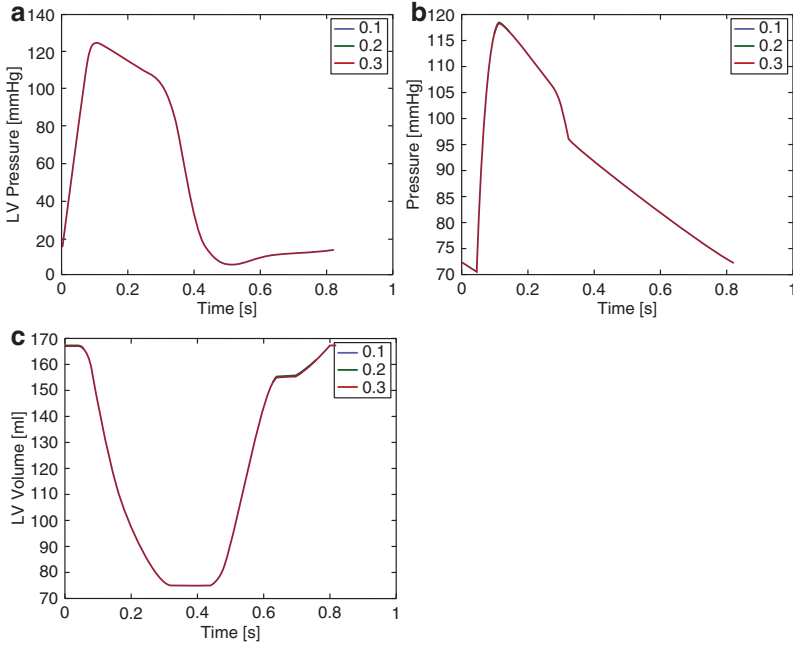


Fig. 5.32 Effect of tricuspid valve inertance on (a) LV pressure, (b) aortic pressure, (c) LV volume. Inertance is expressed in [cm²/s]

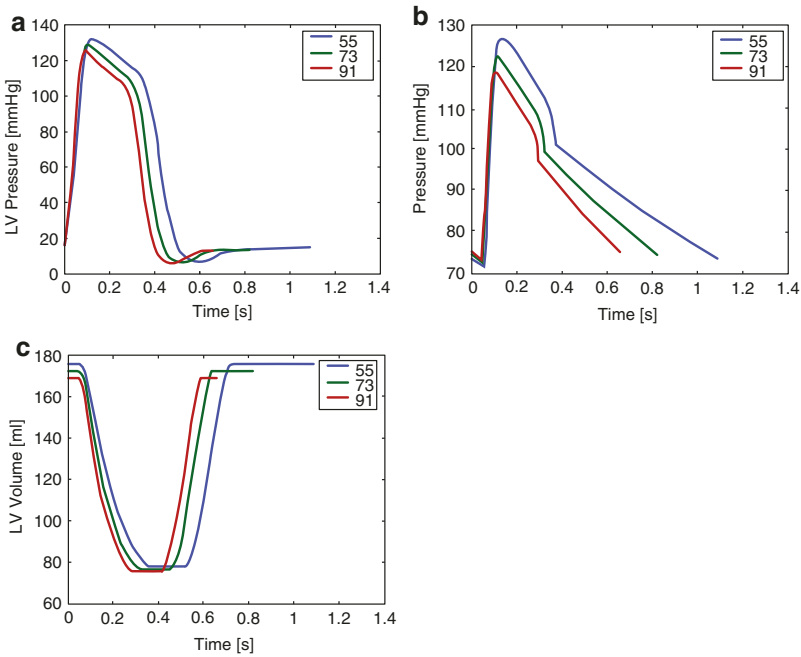


Fig. 5.33 Effect of heart rate on (a) LV pressure, (b) aortic pressure, (c) LV volume. Heart rate is expressed in rpm

5.3.2 Personalization

A set of 12 basic objectives are defined, six for the systemic circulation and six for the pulmonary circulation:

- Maximum aortic pressure
- Minimum aortic pressure
- Average aortic pressure
- Maximum ventricular volume
- Minimum ventricular volume
- Duration of time interval during which the aortic valve is open

The parameters that need to be adapted so as to match the basic objectives are:

- The initial volume in the closed loop model
- The total resistance of the systemic/pulmonary windkessel model
- The compliance of the systemic/pulmonary windkessel model
- The ratio of proximal to distal resistance for the systemic/pulmonary windkessel model
- Timing of the maximum ventricular elastance
- Dead volume of the ventricle

Beyond the set of 12 objectives, the following advanced objectives are employed (both for the systemic and the pulmonary circulation):

- Pressure based objectives (Fig. 5.34)
 - $Slope_1$: the slope of the systolic pressure during early systole (before the valve opens)
 - P_{Dia} : the ventricular pressure at mid diastole
 - $Slope_2$: the slope of the aortic pressure decay during diastole

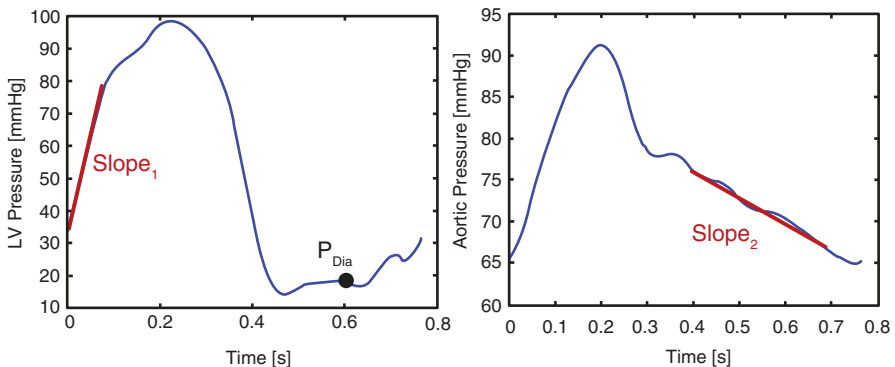


Fig. 5.34 Advanced pressure based objectives

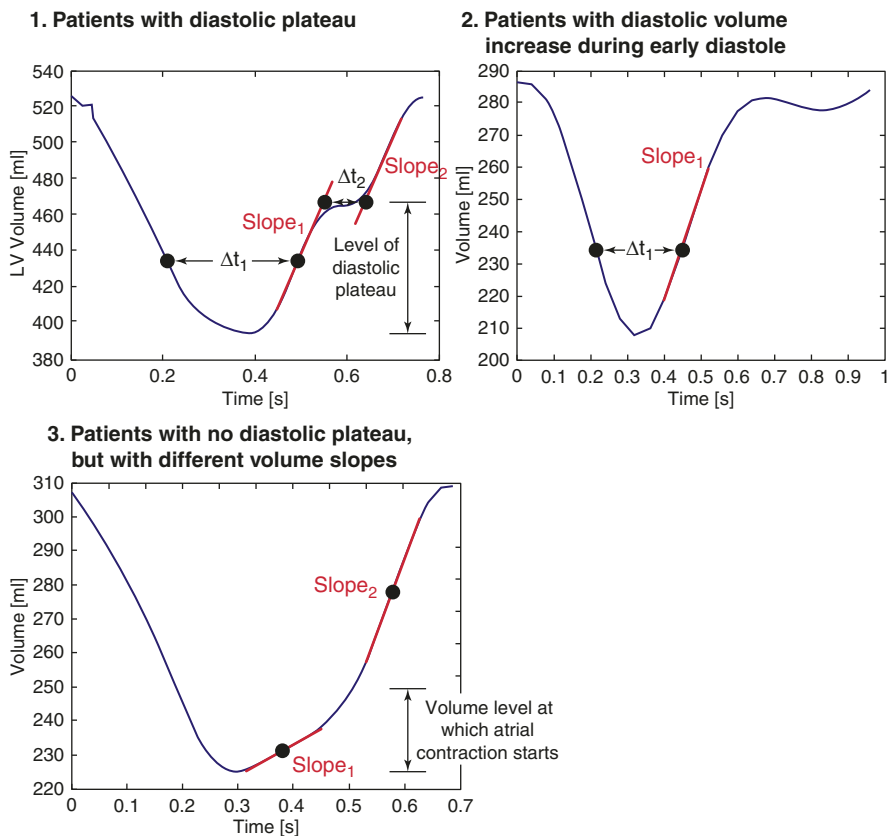


Fig. 5.35 Advanced volume based objectives and classification of patients into three categories

- Volume based objectives: Based on the shape of the volume curve, the patients are classified into three categories (Fig. 5.35).

For the patients with diastolic plateau the following objectives are defined:

- Δt_1 : the delta time on the volume curve between two identical volume values (one in systole and one in diastole), at a volume level of 30% between minimum and maximum volume
- Slope₁: the slope of the volume curve in diastole at the above defined volume value
- Δt_2 : the duration of the diastolic plateau
- Slope₂: the slope of the volume curve when the atrium contracts
- Level of diastolic plateau, expressed in percentages between the min and max volume value

For the patients with diastolic volume increase during early diastole the following objectives are defined:

- Δt_1 : the delta time on the volume curve between two identical volume values (one in systole and one in diastole), at a volume level of 30% between minimum and maximum volume
- $Slope_1$: the slope of the volume curve in diastole at the above defined volume value

For the patients with no diastolic plateau but with different slopes during diastole the following objectives are defined:

- $Slope_1$: the slope of the volume curve in early diastole, before atrial contraction
- $Slope_2$: the slope of the volume curve in late diastole, after atrial contraction
- Volume level at which atrial contraction starts

The parameters that need to be adapted so as to match the advanced objectives are:

- Timing of ventricular elastance curve after maximum elastance is reached
- Mitral/tricuspid valve resistance
- Onset of atrial contraction
- Maximum atrial elastance
- Minimum atrial elastance
- Maximum ventricular elastance
- Minimum ventricular elastance

The personalization is performed as described in Sect. 5.5.2 for the open-loop model.

5.4 Advanced Modeling Aspects

5.4.1 Modeling Valve Regurgitation/Stenosis

The valve model used for the computations described in the following is based on the model previously in Mynard et al. (2012). The main concepts for this valve model are:

- the effective area of the valve is introduced as dynamic variable
- the variation of the area of the valve is determined through a valve state variable, which varies between 0 (closed valve) and 1 (open valve)
- the closure and the opening of the valve are driven by the pressure gradient through the valve
- the model of the valve is a pressure drop model

The model and implementation details are described in detail in the paper mentioned above. Using this type of valve, one can model both healthy and pathologic

states (aortic valve stenosis, aortic valve regurgitation, mitral valve stenosis, mitral valve regurgitation).

In the following some computational results are presented for both healthy and pathologic states, using the open-loop systemic circulation lumped parameter model.

5.4.1.1 Healthy Valves

For the healthy state the following input data was used: SBP = 120 mmHg, DBP = 70 mmHg, HR = 86 bpm, EF = 70%, EDV = 108 ml.

As a result the maximum elastance value of the left ventricle, the systemic compliance and the dead volume of the left ventricle were estimated. The results are displayed in Fig. 5.36.

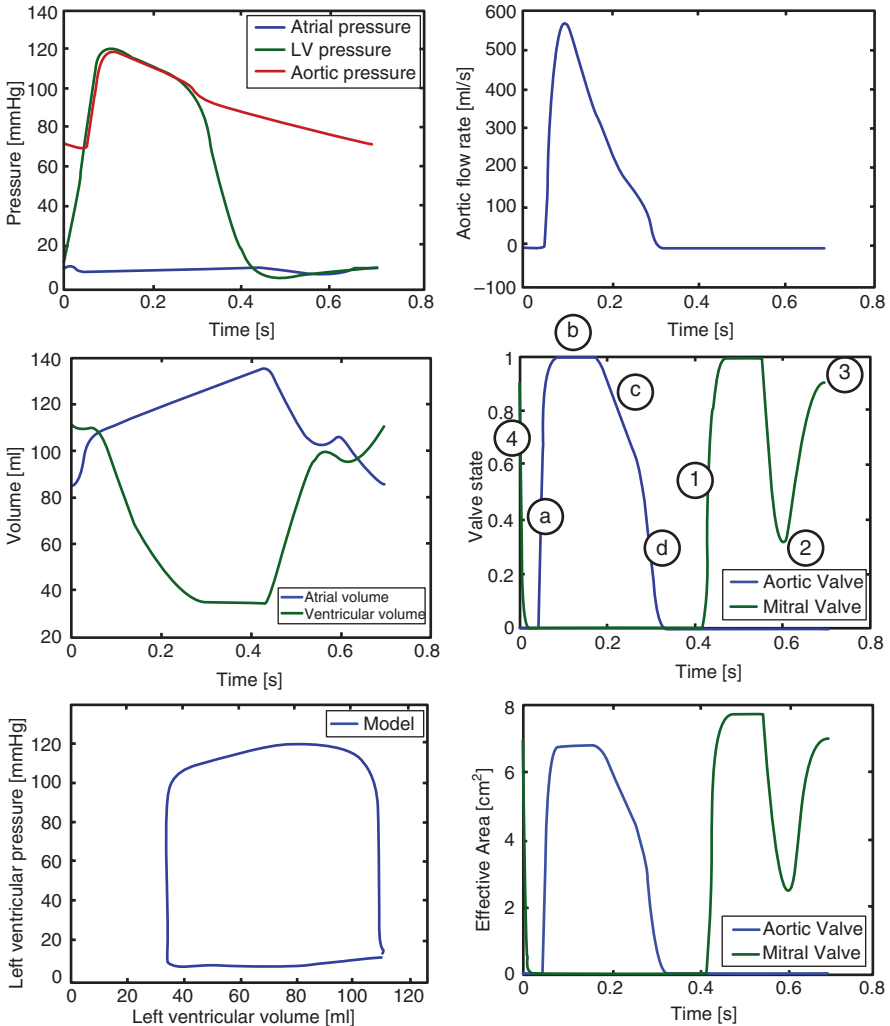


Fig. 5.36 Computational results under healthy conditions

The valve model ensures smooth valve motion (the rate of opening/closure approaches zero as the valve approaches a fully open/closed position). Two constants are used for controlling the speed of valve closure/opening.

Under normal conditions, the **aortic valve** exhibits four phases that have been observed *in vivo* and are predicted by the model: (a) rapid valve opening when LV pressure initially rises above aortic pressure; (b) a short period in which the valve remains fully open; (c) a slow closure phase during the second-half of systole; and (d) rapid closure when the ventricle begins relaxing.

In accord with *in vitro*, experimental and clinical data, the simulated normal **mitral valve** undergoes: (1) rapid opening in early diastole when left ventricular pressure falls below left atrial pressure; (2) partial closure during diastasis when the transmitral pressure difference reverses and then oscillates around zero; (3) full re-opening when left atrial contraction re-establishes a positive pressure gradient; and (4) rapid closure due to left atrial relaxation and left ventricular contraction.

The effective valve area of the aortic and mitral valves varies between a minimum value (0.0 cm^2 under healthy conditions) and a maximum value (6.8 cm^2 for the aortic valve and 7.7 cm^2 for the mitral valve under healthy conditions).

5.4.1.2 Aortic Valve Stenosis

To simulate aortic valve stenosis the maximum effective area of the aortic valve is reduced. The same parameter values as for the healthy state were used and no further tuning was performed.

As displayed in Fig. 5.37, with aortic stenosis, the pressure difference across the aortic valve increases significantly, leading to a much higher LV pressure. Three main changes to valve dynamics are notable with aortic stenosis compared with the normal valve. First, the maximal opening area and rate of opening/closure are reduced as a result of the changes prescribed to the maximum effective area of the aortic valve. Second, the slow closure phase is absent, consistent with clinical findings. Third, although the prescribed time course of the ventricular elastance curve is identical to the healthy case, an increasingly restricted aortic valve leads to progressively longer ejection periods, as has been shown clinically.

The changes in system dynamics are clearly visible in the PV loop, when compared to the healthy case.

5.4.1.3 Aortic Valve Regurgitation

To simulate aortic valve regurgitation the minimum effective area of the aortic valve is increased to a non-zero value. The same parameter values as for the healthy state were used and no further tuning was performed.

As displayed in Fig. 5.38, with aortic regurgitation, one can observe that the aortic flow rate is negative during diastole (as a result of the backflow into the LV). The minimal opening area of the aortic valve is non-zero.

Significant changes are also visible in the PV loop, where the isovolumetric relaxation and contraction phases are missing, due to the fact that the aortic valve is never fully closed.

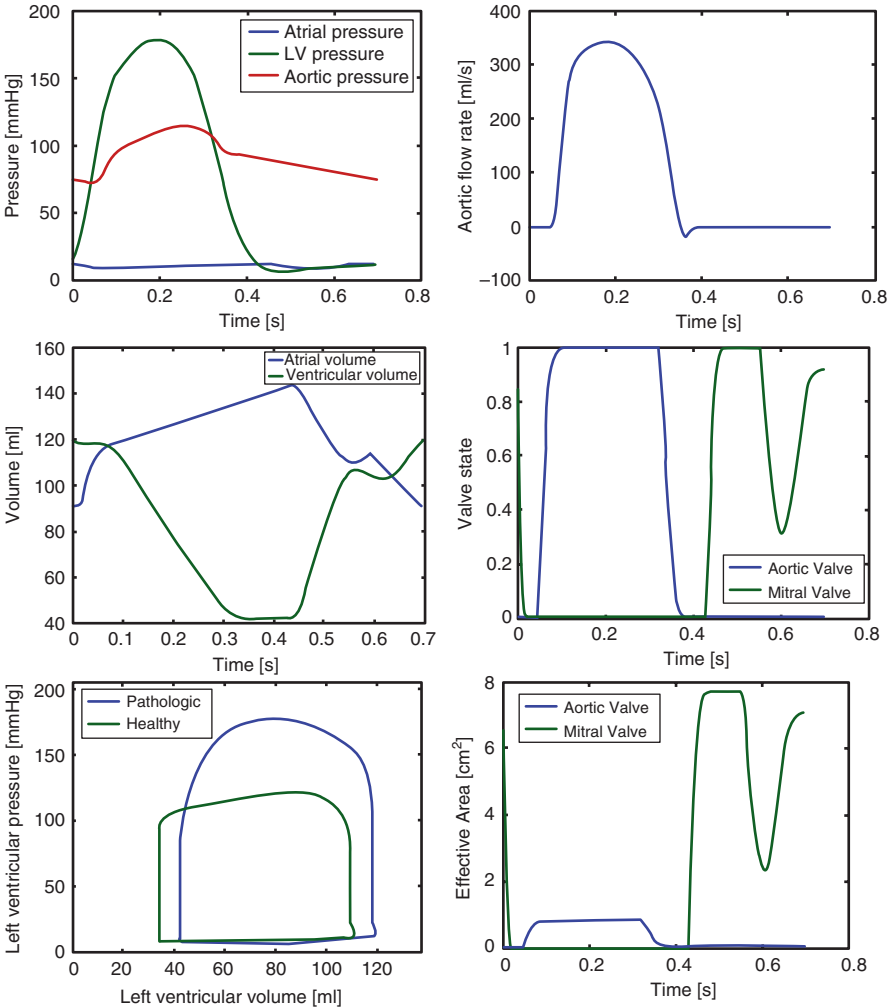


Fig. 5.37 Computational results under aortic valve stenosis

5.4.1.4 Mitral Valve Stenosis

To simulate mitral valve stenosis the maximum effective area of the mitral valve is reduced. The same parameter values as for the healthy state were used and no further tuning was performed.

As displayed in Fig. 5.39, with mitral valve stenosis, atrial volume increases, a restricted mitral valve opening is obtained, and the partial closure phase during diastasis is absent (as has been demonstrated in patients) due to a positive pressure gradient persisting throughout diastole.

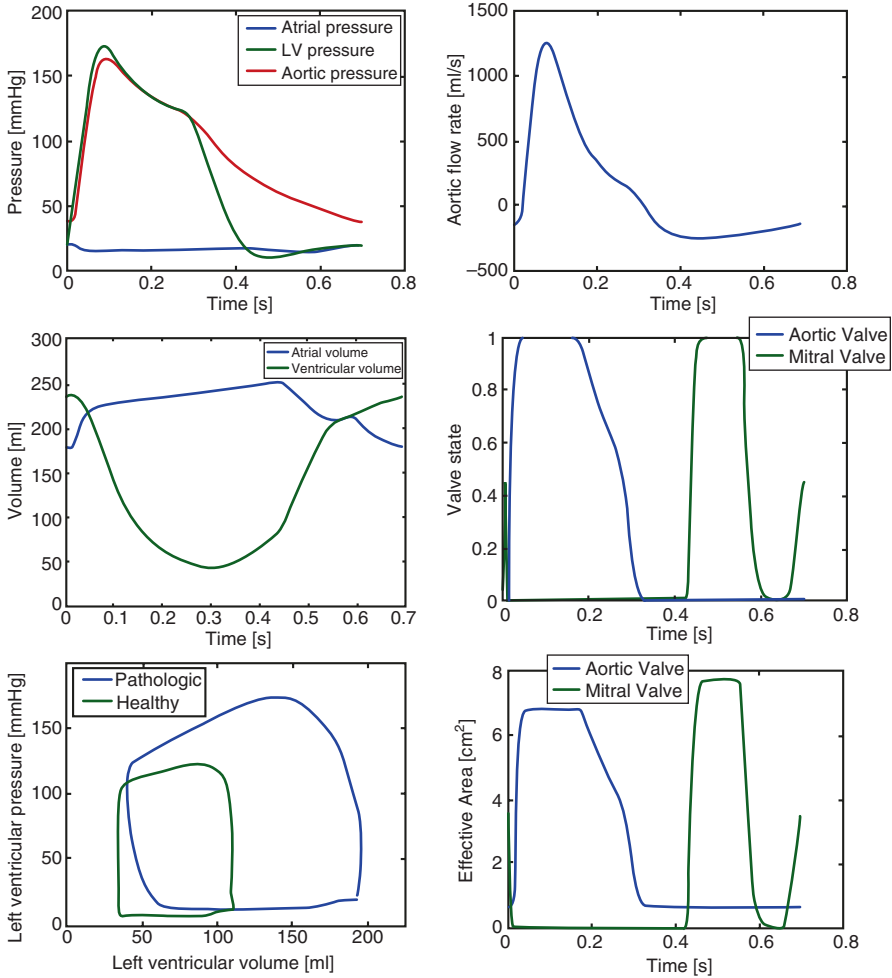


Fig. 5.38 Computational results under aortic valve regurgitation

5.4.1.5 Mitral Valve Regurgitation

To simulate mitral valve regurgitation the minimum effective area of the mitral valve is increased to a non-zero value. The same parameter values as for the healthy state were used and no further tuning was performed.

As displayed in Fig. 5.40, with mitral regurgitation, the minimal opening area of the mitral valve is non-zero. Significant changes are visible in the PV loop, where the isovolumetric relaxation and contraction phases are missing, due to the fact that the mitral valve is never fully closed.

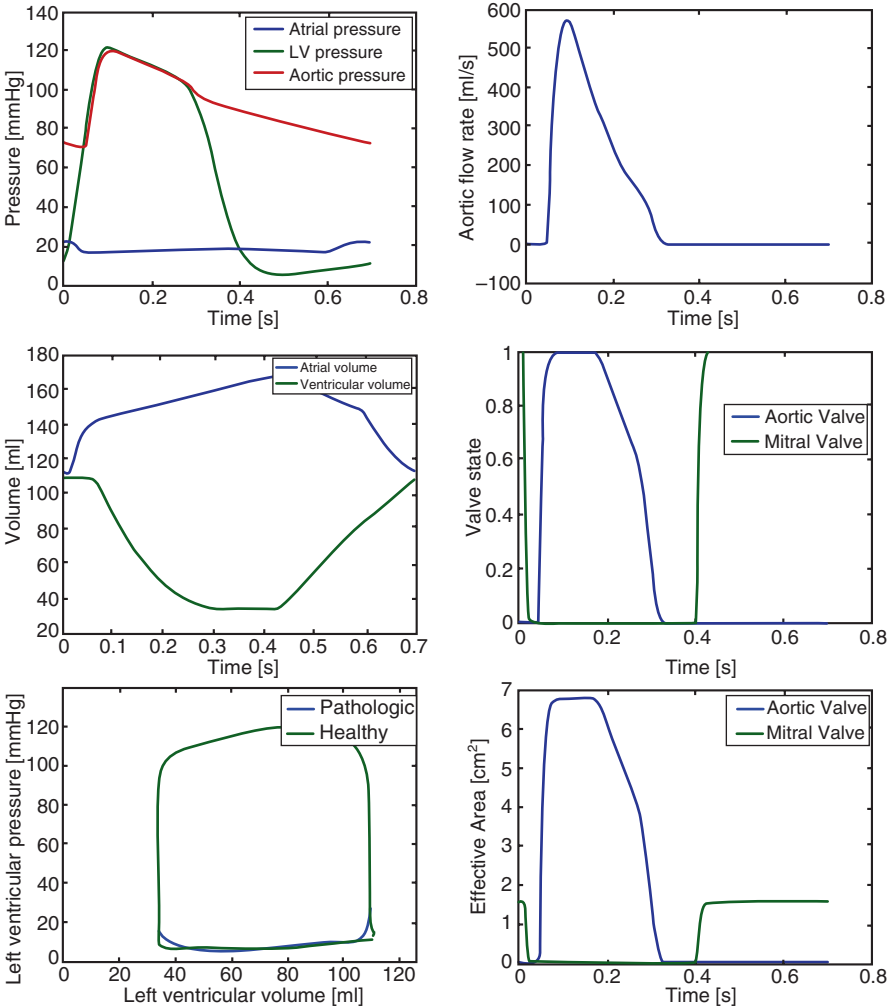


Fig. 5.39 Computational results under mitral valve stenosis

In contrast to the original valve model that was used for computing patient-specific PV loops (composed of a diode, a resistance and an inductance), the herein used valve model is able to compute patient-specific PV loops under pathologic conditions. The main advantage compared to the original valve model is that realistic pressure drop values between the chamber/aorta can be computed.

To be able to compute truly patient-specific results additional patient-specific parameter values are required for the aortic and mitral valve:

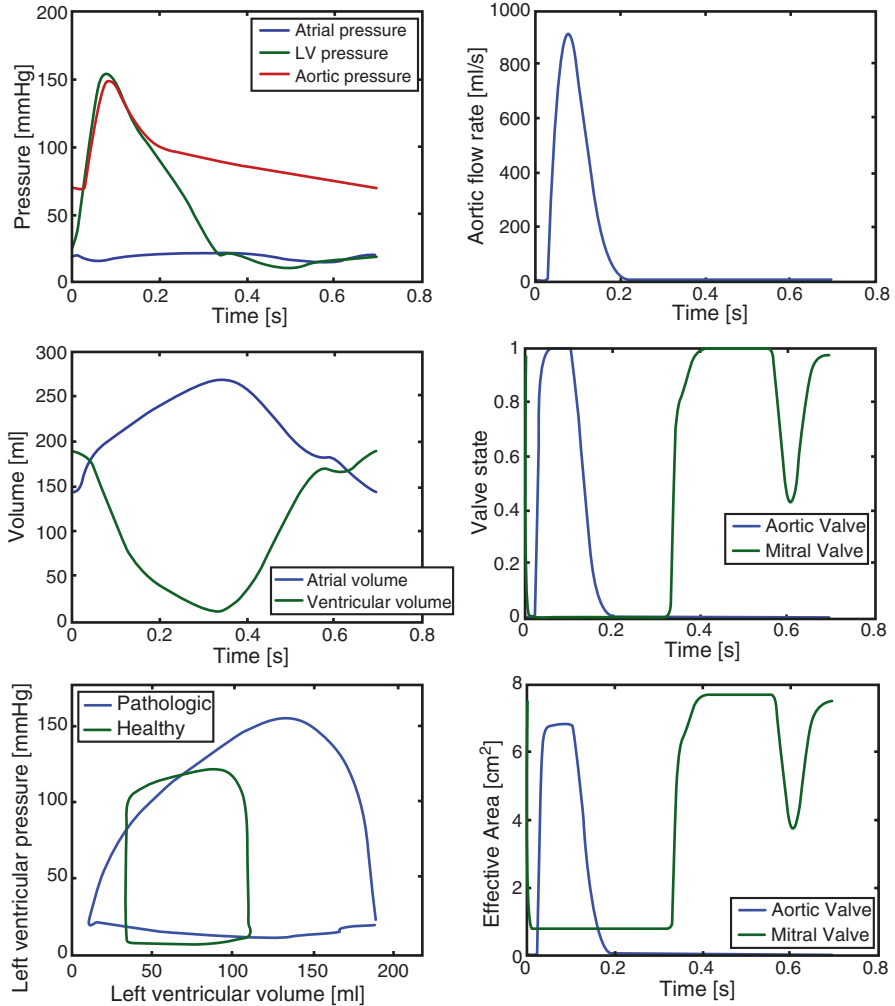


Fig. 5.40 Computational results under mitral valve regurgitation

- maximum annulus area
- minimum annulus area
- dimensions of the LV outflow tract (length and radiuses), dimensions for the ascending aorta (radius)
- information regarding valve opening/closure timing

The original patient-specific values were: SBP, DBP, HR, end diastolic volume, and end systolic volume (or ejection fraction).

5.4.2 Modeling the KG Diaphragm

Another model enhancement is the modeling of the influence of the KG diaphragm on the flow. The KG diaphragm is a soft tissue including the annulus fibrosus and the four heart valves, which undergoes periodic displacement into the atrio-ventricular chambers under the combined action of several forces, including:

- the pressure force due to the pressure difference across the valves and surrounding tissue
- the tissue strain forces from both the atrium and the ventricle sides that act on the base of the annulus fibrosus
- the frictional force from blood flow
- the elastic force due to the elasticity of the KG diaphragm

The KG diaphragm dynamics depends on the balance of all these forces. The MRI measurements of heart kinetics in several heart cycles in an adult native healthy heart show that in the systolic phase the KG diaphragm moves into the ventricular chamber, and in the end diastolic phase it moves into the atrium (due to the atrial contraction). The total displacement along the long axis of the heart is of about 2–3 cm.

The KG diaphragm dynamic equation (for the left heart) is (Korakianitis et al. 2006):

$$M_{sav} \frac{d^2 l}{dt^2} = K_{st, la} \cdot e_{la} - K_{st, lv} \cdot e_{lv} + (P_{lv} - P_{la}) \cdot A_{sav} - K_{f, sav} \frac{dl}{dt} - K_{e, sav} l \quad (5.18)$$

The motion of the KG diaphragm redefines the location of the atrioventricular boundary at each time instant and introduces volume changes to the two left chambers (and similarly to the right cardiac chambers):

$$V_{lv} = V_{lv} + A_{sav} \cdot l \quad \text{and} \quad V_{la} = V_{la} - A_{sav} \cdot l. \quad (5.19)$$

Acknowledgments and Disclaimer The authors would like to thank Bogdan Georgescu, Ali Kamen, Constantin Suci and Dorin Comaniciu for their input.

This feature is based on research, and is not commercially available. Due to regulatory reasons its future availability cannot be guaranteed.

References

- Acierno L (1994) The history of cardiology. The Parthenon Publishing Group, New York
- Burkhoff D (2013) Pressure-volume loops in clinical research: a contemporary view. *J Am Coll Cardiol* 62:1173–1176
- Coogan JS, Pak Chan F, Taylor CA, Feinstein JA (2011) Computational fluid dynamic simulations of aortic coarctation comparing the effects of surgical- and stent-based treatments on aortic compliance and ventricular workload. *Catheter Cardiovasc Interv* 77:680–691

- Dankelmann J, Vergroesen I, Han Y, Spaan JAE (1992) Dynamic response of coronary regulation to heart rate and perfusion changes in dogs. *Am J Phys* 263:447–452
- Drake-Holland AJ, Laird JD, Noble MIM, Spaan JAE, Vergroesen I (1984) Oxygen and coronary vascular resistance during autoregulation and metabolic vasodilation in the dog. *J Physiol* 348:285–300
- Ganong W (1975) Review of medical physiology, 17th edn. Lange Medical Publications, Los Altos
- Guyton A (1991) Textbook of Medical Physiology, 8th edn. W.B. Saunders Company, Philadelphia
- Hall J (2011) Guyton and Hall textbook of medical physiology, 12th edn. Saunders Elsevier, Philadelphia
- Itu L et al (2014) Model based non-invasive estimation of PV loop from echocardiography. In: 36th annual international conference of the IEEE Engineering in Medicine and Biology Society—EMBC 2014, Chicago, August 26–30, pp 6774–6777
- Kim HJ, Jansen KE, Taylor CA (2010) Incorporating Autoregulatory mechanisms of the cardiovascular system in three-dimensional finite element models of arterial blood flow. *Ann Biomed Eng* 38:2314–2330
- Korakianitis T et al (2006) A concentrated parameter model for the human cardiovascular system including heart valve dynamics and atrioventricular interaction. *Med Eng Phys* 28:613–628
- Lakin W et al (2007) Whole-body mathematical model for simulating intracranial pressure dynamics. US 7182602 B2
- Leaning M, Pullen H, Carson E, Finkelstein L (1983) Modelling a complex biological system: the human cardiovascular system-1. Methodology and model description. *Trans Inst Meas Control* 5:71–86
- Miyashiro JK, Feigl E (1995) A model of combined feedforward and feedback control of coronary blood flow. *Am J Phys* 268:895–908
- Mynard JP, Davidson MR, Penny DJ, Smolich JJ (2012) A simple, versatile valve model for use in lumped parameter and one-dimensional cardiovascular models. *Int J Numer Method Biomed Eng* 28:626–641
- Nocedal J, Wright SJ (2006) Numerical optimization, 2nd edn. Springer, New York
- Ottesen J (1997) Nonlinearity of baroreceptor nerves. *Surv Math Ind* 7:187–201
- Ottesen JT et al (2003) Applied mathematical models in human Physiology. Siam Publishing, Philadelphia
- Ottesen JT, Olufsen MS, Larsen JK (2004) Applied mathematical models in human physiology. Siam publications, Philadelphia
- Paeme S et al (2011) Mathematical multi-scale model of the cardiovascular system including mitral valve dynamics. Application to ischemic mitral insufficiency. *Biomed Eng Online* 10:86
- Quarteroni A et al (2001) Coupling between lumped and distributed models for blood flow problems. *Comput Vis Sci* 4:111–124
- Segers P, Stergiopoulos N, Westerhof N, Wouters P, Kolh P, Verdonck P (2003) Systemic and pulmonary hemodynamics assessed with a lumped-parameter heart-arterial interaction model. *J Eng Math* 47:185–199
- Shroff SG, Janicki JS, Weber KT (1985) Evidence and quantitation of left ventricular systolic resistance. *Am J Phys* 249:H358–H370
- Spevack DM, Karl J, Yedlapati N, Goldberg Y, Garcia MJ (2013) Echocardiographic left ventricular end-diastolic pressure volume loop estimate predicts survival in congestive heart failure. *J Card Fail* 19:251–259
- Suga H (1971) Theoretical analysis of a left-ventricular pumping model based on the systolic time-varying pressure/volume ratio. *IEEE Trans Biomed Eng* 18:47–55
- Taher M, Cecchini A, Allen M, Gobran S, Gorman R, Guthrie B, Lingenfelter K, Rabbany S, Rolchigo P, Melbin J, Noordergraaf A (1988) Baroreceptors responses derived from a fundamental concept. *Ann Biomed Eng* 16:429–443
- Tortora G, Anagnostakos N (1990) Principles of anatomy and physiology, 6th edn. Harper and Row Publishers, New York
- Ursino M (1999) A mathematical model of the carotid-baroreflex control in pulsatile conditions. *IEEE Trans Biomed Eng* 46:382–392

-
- Ursino M (2000) Modelling the interaction among several mechanism in the short-term arterial pressure control. In: Danielsen M, Ottesen J (eds) *Mathematical Modelling in Medicine*. IOS Press, Amsterdam, pp 139–162
- Van Slochteren FJ, Grundeman PF, Teske AJ, Bovendeerd PHM (2012) Left ventricular PV loop estimation using 3D echo. Eindhoven University of Technology, Internal Report BMTE 07.42. <http://www.mate.tue.nl/mate/pdfs/8738.pdf>.